CHALMERS
UNIVERSITY OF TECHNOLOGY

Collaborative scheduling of shared electric vehicle charging stations

Transportation Research Part D 156 (2026) 105391

Contents lists available at ScienceDirect

Transportation Research Part D

journal homepage: www.elsevier.com/locate/trd

Collaborative scheduling of shared electric vehicle charging stations

Fangting Zhou [a,*], Balázs Kulcsár [b], Jiaming Wu [a]

[a] Architecture and Civil Engineering, Chalmers University of Technology, Gothenburg, Sweden
[b] Electrical Engineering, Chalmers University of Technology, Gothenburg, Sweden

ARTICLE INFO

Keywords:
Urban logistics
Collaborative scheduling
Electric vehicle
Shared charging
Balanced bounding box method
Nash bargaining

ABSTRACT

Electric vehicle charging faces challenges of high infrastructure costs and low utilization. Shared charging among fleet operators offers a sustainable alternative. This study formulates a collaborative scheduling problem in which two companies coordinate charging to minimize their individual costs while achieving efficient and equitable outcomes. A bi-objective optimization framework is developed, proposing the Balanced Bounding Box Method (B3M) to generate a representative subset of globally optimal solutions with substantially reduced computational effort. Cooperative bargaining is then applied to derive an actionable final decision from the efficient frontier. Numerical results show that this framework maintains frontier integrity while cutting computation time. Beyond improving decision efficiency, the study offers insights into how transparent and equitable solution selection can sustain long-term collaboration among operators. The framework provides practical guidance to improve charger utilization and reduce system costs, supporting more sustainable use of existing infrastructure.

1. Introduction

Electric vehicles (EVs) are widely recognized as a key solution for decarbonizing transportation, offering up to 50% lower greenhouse gas emissions and reduced energy consumption compared to gasoline vehicles (Kumar et al., 2021). As a result, global EV adoption is accelerating rapidly. This trend is reflected in the global EV stock, which exceeded 60 million in 2024 and is expected to continue growing under current policy settings (IEA, 2025). This surge places unprecedented pressure on charging infrastructure, especially public charging networks, which are expected to expand significantly to support this growth and play a critical role in promoting EV adoption and emissions reduction (Levinson and West, 2018; Bauer et al., 2021). Yet, ensuring the economic viability of these networks remains a persistent challenge.

More specifically, expanding public charging infrastructure remains a costly and complex endeavor, involving substantial investment in installation, maintenance, and grid upgrades (ACEA, 2022). Public-access charging is typically more expensive than home or depot-based charging, imposing a higher cost burden on users such as fleet operators (Kampshoff et al., 2022; European Alternative Fuels Observatory, 2024). Moreover, low utilization rates further undermine economic viability. In 2022, public fast-charging stations in the U.S. averaged only 7.5% utilization, far below the 15% threshold typically required for financial feasibility (Fröde et al., 2023). While expanding public charging infrastructure remains essential, evidence suggests that physical growth alone cannot ensure efficient or reliable access (Liu et al., 2023b). In particular, the performance of charging networks is often limited by plan-

* Corresponding author.
E-mail address: fangting@chalmers.se (F. Zhou).

https://doi.org/10.1016/j.trd.2026.105391
Received 30 October 2025; Received in revised form 15 April 2026; Accepted 15 April 2026
Available online 29 April 2026

ning inefficiencies, operational limitations, and user behavior (Yi et al., 2022; Liu et al., 2023a; Chen et al., 2024). These challenges motivate the development of smarter scheduling strategies aimed at improving utilization and cost-effectiveness.

In response to these challenges, shared charging has emerged as a promising approach to improve infrastructure efficiency and reduce cost burden by enabling multiple users to access the same facilities. Recent studies show that such models not only increase station utilization but also generate additional revenue for infrastructure owners (Gao et al., 2021; Melander and Wallström, 2023; Cai et al., 2024). Platforms like Share&Charge and Co Charger have adopted this concept, allowing individuals and businesses to rent out underutilized chargers via digital marketplaces (Vanrykel et al., 2018; Co Charger, 2025). Moreover, the adoption of booking-based systems by several charging networks (e.g., EVgo, GO TO-U) enable users to reserve charging slots in advance (EVgo Press Office, 2021; ABB News Center, 2021), facilitating coordinated access to shared charging resources.

Existing research on shared charging primarily focuses on pricing strategies and market mechanisms for revenue generation. For example, Gao et al. (2021) propose an auction-based pricing model, while Cai et al. (2024) develop a ride-sourcing charger-sharing program. Other studies examine cross-fleet sharing between electric buses and private EVs, showing that coordinated scheduling can improve utilization and economic benefits (Ji et al., 2023; Jia et al., 2024). Meanwhile, fleet-based EV scheduling has been extensively studied, with some work adopting multi-objective models (Hajforoosh et al., 2015; Wu et al., 2020), but these studies primarily focus on optimizing individual fleet operations rather than coordinating access to shared charging infrastructure. Moreover, existing studies typically rely on a centralized or dominant operator and do not fully capture coordination among multiple self-interested users, including competing user demands, scheduling conflicts, cost allocation, and fairness in shared charging systems.

Despite their potential, shared charging systems face operational challenges due to multi-user interactions and limited scheduling resources. Most models optimize single-user objectives and lack cooperative mechanisms. In practice, coordinating access while balancing efficiency and fairness across multiple stakeholders remains challenging, which limits the effectiveness and practical applicability of existing frameworks. Addressing these challenges is essential to fully realize the full potential of shared charging infrastructure.

To bridge this gap, this study investigates EV charging scheduling in shared charging environments with multiple independent operators coordinating access to common charging infrastructure. The goal is to improve cost efficiency while mitigating operational conflicts arising from competition for limited charging resources. Such settings naturally give rise to strategic interactions between operators, requiring coordination to balance efficiency and fairness in resource allocation. Accordingly, we adopt a collaborative scheduling perspective that emphasizes joint decision-making under competing objectives, providing a foundation for coordination mechanism design in shared charging systems.

Building on this framework, we introduce a bi-objective optimization model integrated with game theory, where two operators pursue cost-minimization objectives while coordinating access to shared charging infrastructure. The model jointly optimizes two interconnected decisions: (i) determining which charging stations each company should rent, and (ii) coordinating the scheduling of charging activities across the shared network. To efficiently solve the bi-objective optimization model, we develop the Balanced Bounding Box Method (B3M), which delineates the non-dominated frontier by filtering out closely positioned solutions to generate a compact and representative subset, thereby improving computational efficiency and solution diversity. In addition, the framework integrates cooperative bargaining mechanisms to model strategic interactions between companies, guiding them toward mutually beneficial agreements that effectively manage trade-offs in their competing objectives. Numerical case studies demonstrate the computational efficiency and effectiveness of the proposed approach while maintaining high solution quality.

The main contributions of this paper are as follows:

- We study EV charging scheduling from a collaborative perspective involving independent fleet operators, focusing on coordination challenges and conflicts arising from shared charging resources.
- We develop a bi-objective integer programming formulation, where each company minimizes its own costs within a shared charging environment, departing from existing centralized or single-operator charging models.
- To efficiently solve the resulting bi-objective problem, we propose a novel Balanced Bounding Box Method (B3M) to identify a compact and well-distributed set of non-dominated solutions without exhaustive enumeration of the frontier.
- Unlike most existing studies that stop at generating non-dominated solutions, we explicitly bridge multi-objective optimization and actionable decision-making by incorporating cooperative bargaining mechanisms to support the selection of a fair and implementable mutually agreed final operating solution from the non-dominated set.

The remainder of this paper is organized as follows. Section 2 reviews the relevant literature. Section 3 outlines the problem and formulates the mathematical programming model. Section 4 develops the B3M to identify non-dominated solutions and presents two cooperative bargaining methods for determining the final agreement point. Section 5 presents the experimental study and numerical results. Section 6 discusses the main findings and insights of the study. Finally, Section 7 concludes the paper and suggests directions for future research.

2. Literature review

This section reviews existing studies related to shared charging, EV charging scheduling, and relevant solution methods, with a focus on collaborative charging settings.

Shared charging stations

Research on shared charging infrastructure has attracted growing attention as a way to improve charger utilization and reduce costs. Existing studies mainly focus on market-based and pricing mechanisms to support charger sharing. For example, Gao et al. (2021) propose a double-auction-based market for sharing underutilized chargers, and Cai et al. (2024) study platform-based sharing programs that optimize pricing and market outcomes across multiple stakeholders.

Beyond pricing-oriented approaches, Melander and Wallström (2023) examine horizontal B2B collaboration in sharing charging infrastructure for electric freight vehicles, identifying multiple business models for sharing and highlighting the importance of trust, data sharing, and coordination among participating companies. Their findings demonstrate that shared charging can bring both economic and environmental benefits, while also revealing the organizational and collaborative challenges inherent in such horizontal networks.

A few studies consider operational aspects of shared charging. Ji et al. (2023), for instance, integrate electric bus scheduling with charging facility sharing by allowing electric cars to access bus chargers during specified time windows. However, such models typically assume a single dominant operator or centralized decision-making and do not explicitly address conflicts or coordination among multiple independent users.

Overall, despite growing interest in shared charging, existing research remains largely centered on pricing and business structures, with limited attention to scheduling-based coordination mechanisms that ensure fairness, resolve conflicts, and support collaboration among multiple competing users.

EV charging scheduling

EV charging scheduling has been widely studied under various operational settings, including different station configurations and pricing mechanisms (Zhang et al., 2018). Most existing studies focus on centralized scheduling, typically from the perspective of a single operator, aiming to minimize charging costs, reduce peak load, or maximize user utility. For example, Wei et al. (2017) study EV charging scheduling in parking garages under time-of-use pricing, and Wu et al. (2020) propose a time-slotted scheduling model to reduce charging costs and peak demand. While some studies adopt multi-objective optimization to balance conflicting goals, these models are typically formulated from the perspective of a single decision-maker and do not explicitly capture strategic interactions among multiple independent stakeholders (Zakariazadeh et al., 2014; Hajforoosh et al., 2015; Wu et al., 2020).

In contrast, collaborative scheduling among multiple operators has received limited attention, particularly in horizontal settings where companies share charging infrastructure. These gaps highlight the need for collaborative charging scheduling frameworks that support coordination among multiple independent operators while accounting for individual costs and fairness.

Solution methods

In horizontal collaboration among EV fleet operators, charging schedules naturally involve conflicting objectives across different stakeholders, making multi-objective optimization a suitable modeling framework. Multi-objective optimization aims to identify efficient trade-offs among conflicting objectives (Laidoui et al., 2023). However, practical collaborative decision-making typically requires selecting a single implementable solution from these alternatives. To this end, some studies have combined multi-objective optimization with game-theoretic or bargaining-based mechanisms to facilitate coordination and reach mutually acceptable final decisions.

Most research on multi-objective charging scheduling, like many other optimization problems, relies on decision space search algorithms. For example, fuzzy genetic algorithms and fuzzy discrete particle swarm optimization have been used to coordinate the charging of PEVs (Hajforoosh et al., 2015). More generally, classical evolutionary algorithms such as genetic algorithms, differential evolution, and particle swarm optimization have been widely applied to address EV charging scheduling problems (Wu et al., 2017; Yin et al., 2021). However, these decision space search algorithms often lack guarantees of global optimality and robustness, motivating the use of criterion space search methods that provide more controlled exploration of optimal solutions.

In contrast, few studies have explored multi-objective EV charging using criterion space search algorithms, such as the augmented ϵ-constraint method (Zakariazadeh et al., 2014; Das et al., 2020), which typically focus on identifying subsets of non-dominated solutions rather than the entire solution set. In addition to the ϵ-constraint method, commonly used criterion space search methods include the weighted sum method, perpendicular search method, and augmented weighted Tchebycheff method. These methods operate by converting a multi-objective optimization problem into a series of single-objective problems, which are then solved sequentially. As a representative criterion space search approach, the balanced box method decomposes the criterion space and has demonstrated effectiveness in various bi-objective optimization problems (Boland et al., 2015; Wang et al., 2020; Smet, 2023). Building on this, some studies have proposed extensions of the balanced box method. For example, Dai and Charkhgard (2018) introduced a two-stage approach that combines the balanced box method with the ϵ-constraint method to solve a smaller set of single-objective integer linear programs.

While both decision space search and criterion space search methods have been widely adopted for multi-objective EV charging scheduling, existing studies typically emphasize either heuristic-based exploration of solution sets or exact characterization of Pareto fronts. However, few works explicitly address how to support the selection of an implementable decision from the non-dominated set while retaining the optimality guarantees offered by exact optimization techniques.

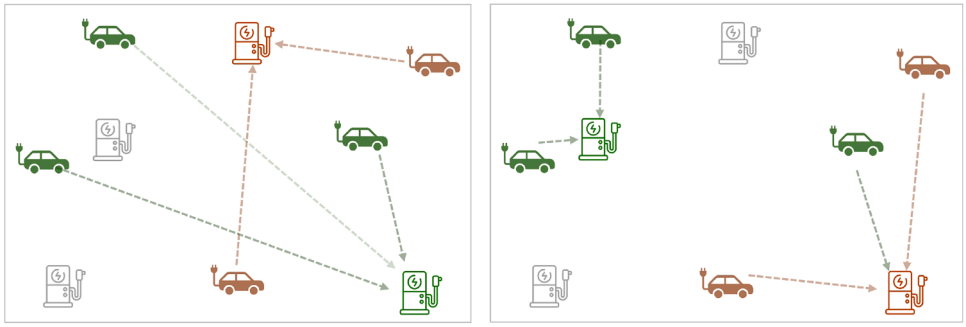

Fig. 1. Schematic illustration of the collaborative charging scheduling problem.

This limitation is particularly critical in shared charging systems involving multiple independent operators, where practical deployment requires not only identifying efficient trade-offs but also enabling coordinated, fair, and computationally efficient decision-making among stakeholders. These gaps motivate the need for solution frameworks that integrate multi-objective optimization with coordination mechanisms in collaborative charging environments.

3. Bi-objective integer programming model

3.1. Problem description

This study examines the collaborative scheduling problem where two fleet operators rent and share dedicated charging facilities from a third party to exclusively serve their EV fleets. The goal is to jointly optimize charging station rental decisions and charging schedules while minimizing each operator's operational cost and ensuring fair resource allocation. The system setting is schematically illustrated in Fig. 1.

In this setting, the two companies (i.e., the fleet operators, represented in green and orange) have access to four charging stations available for rent. Fig. 1 (a) depicts the non-collaborative scenario, where each charging station is exclusively used by a single company. In contrast, Fig. 1 (b) illustrates the collaborative scenario, where EVs from both companies can utilize all charging stations within the coalition. By sharing charging resources, the collaboration is expected to lower costs, improve utilization, and provide greater scheduling flexibility.

The core challenge lies in coordinating these interdependent decisions across multiple operators in a way that balances their individual cost objectives and enables fair and coordinated decision-making. Each company seeks to minimize its own costs, including station rental fees, electricity costs, energy consumption for traveling to the station, and waiting time due to scheduling constraints. These objectives naturally lead to a bi-objective optimization problem, where solutions form an efficient frontier capturing trade-offs between operators' costs. To ensure equitable resource distribution, a cooperative bargaining mechanism is introduced, guiding companies toward a fair and cost-effective solution.

The problem formulation incorporates multiple constraints to ensure feasible and consistent rental and scheduling decisions: (i) charging continuity constraints, ensuring uninterrupted charging sessions, (ii) charger capacity constraints, limiting simultaneous usage per station, (iii) charging time constraints, defining valid scheduling windows, (iv) charging demand and capacity constraints, ensuring sufficient energy supply for each EV, and (v) charger rental constraints, ensuring each station is rented by only one company and used accordingly.

3.2. Model setup and notations

We consider a collaborative EV charging scenario in which multiple fleet operators coordinate the use of a set of third-party charging stations via a centralized scheduling platform. This structure reflects an emerging operational model in urban logistics and shared mobility systems, where vehicles from different companies access charging infrastructure under rental agreements and negotiated usage rules.

In such systems, the next day's operational plans and vehicle assignments are typically determined in advance. Many charging networks, especially those serving commercial fleets, operate under booking-based systems, where users or vehicles pre-reserve charging slots to ensure station availability and reduce waiting times. Fleet operators use telematics and battery monitoring systems to estimate charging needs and submit them to the platform prior to scheduling. Charging demand, including energy requirements, time windows, and location preferences, is assumed to be known, as it is typically derived from upstream planning processes such as route planning and battery monitoring. This reflects the scheduling-level focus of the proposed model. Based on these inputs, the platform determines which vehicles are granted access to which stations, during which time intervals, and under what pricing terms.

Table 1
Mathematical notation.

Sets:	
I	Set of EVs, $i \in I$
J	Set of chargers, $j \in J$
K	Set of companies, $k \in K$
T	Set of time intervals, $\tau \in T$
I_k	Set of EVs of company k, $I_k \subset I$
Parameters:	
$f_{j,k}$	Fixed rental fee of charger j for company k
$c_j^{c,\tau}$	Unit energy fee for collaborative EVs charging at charger j in time interval τ
$c_j^{o,\tau}$	Unit energy fee for own EVs charging at charger j in time interval τ
λ_i	Value of time of EV i
ε_{ij}	Charging rate of EV i at charger j
w_{ij}	Energy cost for EV i travels to charger j
$[e_i, l_i]$	Available charging time window of EV i
$[L_i, H_i]$	Maximum and minimal charging amount of EV i
Decision variables:	
x_{ij}^{τ}	1 if charger j serves EV i in time interval τ, 0 otherwise
$y_{j,k}$	1 if charger j is rented by company k, 0 otherwise
Auxiliary variables:	
$u_{ij,k}^{\tau}$	A binary variable is introduced to linearize the product of x_{ij}^{τ} and $y_{j,k}$.
t_i^s, t_i^f	Start and end charging time of EV i
$\underline{x_{ij}^{\tau}}$, $\overline{x_{ij}^{\tau}}$	1 if EV i starts (concludes) charging at charger j during time interval τ, 0 otherwise.

Charging station usage involves two types of cost: rental and electricity fees. A company that leases a station is responsible for the corresponding rental fee and electricity cost incurred when its own EVs are charged. Under centralized coordination, the use of a leased station may be shared: if a vehicle from another participating company is scheduled to use that station, it is charged a collaborative electricity price determined by the platform. Electricity prices may vary by user type, station, and time interval. To reflect physical capacity constraints, each charger is restricted to serving a single EV per time slot in the model.

The scheduling horizon is discretized into equal-length time intervals. Vehicles can only be assigned to contiguous time slots, and their total charging duration must be sufficient to meet their demand. Moreover, we assume that once charging begins, it must be uninterrupted until the energy demand is satisfied. This reflects typical operational constraints, such as physical plug-locking mechanisms or platform-imposed charging continuity rules.

Given these assumptions and modeling setups in place, we introduce decision variables for charging station rental and EV scheduling. Specifically, $y_{j,k}$ indicates whether company k rents charger j, while x_{ij}^{τ} represents whether EV i is assigned to charger j during time interval τ. In addition, time-related variables, such as t_i^s and t_i^f, are introduced to represent the start and end times of each EV's charging session, ensuring proper scheduling coordination. The notations used in this study, including decision variables, auxiliary variables, parameters, and sets, are summarized in Table 1 for reference. To formally define the optimization problem, we distinguish between predefined input parameters and optimization decision variables. The input parameters include the set of EVs I, chargers J, companies K, and time intervals T, along with parameters such as charging rates, energy fees, rental cost, and vehicle-specific charging demands. The decision variables include charging station rental decision ($y_{j,k}$) and EV charging schedules (x_{ij}^{τ}), while auxiliary variables facilitate scheduling coordination and maintain model tractability. These elements collectively define the bi-objective integer programming model presented in Section 3.3.

With these definitions in place, the following section presents the mathematical formulation of the problem, ensuring that all rental and scheduling decisions satisfy the defined constraints.

3.3. Model formulation

The problem is formulated as a bi-objective integer programming model, where all decision variables are integers. This formulation jointly optimizes station rental and scheduling decisions across operators. The model comprises two distinct objective functions, each representing the cost-minimization goal of a company.

(I) Objective function

The objective function is formulated as:

$$\min_{(x_{ij}^{\tau}, y_{j,k}) \in \mathcal{X}} \left(z_k(x_{ij}^{\tau}, y_{j,k}) \mid k = 1, 2 \right). \tag{1}$$

In Eq. (1), $z_k(x_{ij}^{\tau}, y_{j,k})$ represents the costs incurred by company k. These costs are comprised of several sources, including rental fees, electricity charges (from EV charging), energy consumption (from travel), and time costs. It is defined as follows:

$$z_k(x_{ij}^{\tau}, y_{j,k}) = \sum_{j\in J} \mathrm{f}_{j,k} y_{j,k} + \sum_{i\in I_k}\sum_{j\in J}\sum_{\tau\in T}\left(\sum_{k'\in K,\, k'\neq k} \mathrm{c}_j^{\mathrm{c},\tau} y_{j,k'} + \mathrm{c}_j^{\mathrm{o},\tau} y_{j,k}\right)\varepsilon_{ij} x_{ij}^{\tau} + \sum_{i\in I_k}\sum_{j\in J}\sum_{\tau\in T} w_{ij}\, \underline{x_{ij}^{\tau}} + \sum_{i\in I_k} \lambda_i\left(t_i^{\mathrm{s}} - e_i\right) \tag{2}$$

where the first term represents the rental fee, which is determined by the fixed unit cost, represented by $\mathrm{f}_{j,k}$, for the rented charging stations. The second term denotes the charging fee. The unit charging fee for collaborative EVs and own EVs is represented by $\mathrm{c}_{\mathrm{c},j}^{\tau}$ and $\mathrm{c}_{\mathrm{o},j}^{\tau}$, respectively. Moreover, the variable ε_{ij} represents the charging rate. The third term is the energy consumption cost from the EV to the charging station, with the energy consumption matrix represented by w_{ij}. The final term represents the opportunity cost associated with waiting time for charging. This can be calculated by multiplying the drivers' value of time (λ_i) by the waiting time ($t_i^{\mathrm{s}} - e_i$). It should be noted that electricity fees may vary depending on location and time, and may differ between charging the company's own EVs and those of the other company.

In this model, the two objectives are addressed separately, rather than being combined into a single weighted sum. This approach yields a **non-dominated frontier** also referred to as the **efficient frontier**, wherein the advancement of one objective entails a detriment to the other. The efficient frontier offers a means of reconciling the two companies' goals, a process that will be further elucidated in Section 4.

(II) Charging continuity constraints

To ensure uninterrupted charging, two additional auxiliary variables, denoted by $\underline{x_{ij}^{\tau}}$ and $\overline{x_{ij}^{\tau}}$, are introduced. If the value of $\underline{x_{ij}^{\tau}}$ is equal to 1, this signifies that EV i starts the charging process at charger j within the specified time interval τ, as defined in:

$$\underline{x_{ij}^{\tau}} \geq \begin{cases} x_{ij}^{\tau} - x_{ij}^{\tau-1}, & \tau = 2,3,4\ldots,\mathscr{T} \\ x_{ij}^{\tau}, & \tau = 1. \end{cases} \forall i \in I, j \in J \tag{3}$$

Similarly, if the value of $\overline{x_{ij}^{\tau}}$ is equal to 1, this denotes that EV i has completed the charging process at charger j within the time interval τ, as given by:

$$\overline{x_{ij}^{\tau}} \geq \begin{cases} x_{ij}^{\tau} - x_{ij}^{\tau+1}, & \tau = 1,2,3\ldots,\mathscr{T}-1 \\ x_{ij}^{\tau}, & \tau = \mathscr{T}. \end{cases} \forall i \in I, j \in J \tag{4}$$

(III) Charging location constraints

Each EV is constrained to charging at a single charger only once, and these limitations can be expressed as:

$$\sum_{\tau\in T}\sum_{j\in J} \underline{x_{ij}^{\tau}} = 1, \forall i \in I, \tag{5}$$

$$\sum_{\tau\in T}\sum_{j\in J} \overline{x_{ij}^{\tau}} = 1, \forall i \in I, \tag{6}$$

and

$$\sum_{\tau\in T} \underline{x_{ij}^{\tau}} = \sum_{\tau\in T} \overline{x_{ij}^{\tau}}, \forall i \in I, j \in J. \tag{7}$$

(IV) Charger capacity constraints

Each charger is limited to charging one EV per time interval, as expressed by:

$$\sum_{i\in I} x_{ij}^{\tau} \leq 1, \forall j \in J, \tau \in T. \tag{8}$$

(V) Charging time constraints

The start charging time t_i^{s} and end charging time t_i^{f} are also auxiliary variables that can be represented by:

$$t_i^{\mathrm{s}} = \sum_{\tau\in T}\sum_{j\in J} \underline{x_{ij}^{\tau}}(\tau - 1), \forall i \in I, \tag{9}$$

$$t_i^{\mathrm{f}} = \sum_{\tau\in T}\sum_{j\in J} \overline{x_{ij}^{\tau}}\tau, \forall i \in I, \tag{10}$$

and

$$\sum_{\tau\in T}\sum_{j\in J} x_{ij}^{\tau} = t_i^{\mathrm{f}} - t_i^{\mathrm{s}}, \forall i \in I. \tag{11}$$

To clarify the representation of the charging duration, the start charging time t_i^{s} is defined to occur between 0 and $\mathscr{T} - 1$, while the end charging time t_i^{f} occurs between 1 and $\mathscr{T}$. The total charging duration is calculated as the difference between the end charging

time t_i^{f} and the start charging time t_i^{s}. For example, if charging takes place during the interval τ, the start time is $\tau - 1$, and the end time is τ, resulting in a charging duration of one time unit.

The start and end of charging are constrained by the predetermined time windows for each EV:

$$e_i \le t_i^{\mathrm{s}} \le t_i^{\mathrm{f}} \le l_i, \forall i \in I. \tag{12}$$

(VI) Charging demand and capacity constraints

The minimum and maximum requirements limit the amount of charge for each EV:

$$L_i \le \sum_{j\in J}\sum_{\tau\in T} \varepsilon_{ij} x_{ij}^{\tau} \le H_i, \forall i \in I, \tag{13}$$

where the charging rate, denoted as ε_{ij}, represents the charging rate of EV i when using charger j. L_i and H_i are the lower and upper bounds of the charging demand of EV i.

(VII) Charger rental constraints

Each charger can be rented by a maximum of one company, as constrained by:

$$\sum_{k\in K} y_{j,k} \le 1, \forall j \in J. \tag{14}$$

Furthermore, EVs can only be served by a charger if it is rented, expressed as:

$$x_{ij}^{\tau} \le \sum_{k\in K} y_{j,k}, \forall i \in I, j \in J, \tau \in T. \tag{15}$$

With these constraints, the problem formulation is complete.

To simplify the solution process for the proposed model, the objective function is linearized. An auxiliary binary variable, $u_{ij,k}^{\tau}$, is introduced to replace the nonlinear term $x_{ij}^{\tau} y_{j,k}$. This transformation enables the use of standard integer linear programming techniques. The following constraints are introduced to ensure the linearization accurately captures the relationship between x_{ij}^{τ}, $y_{j,k}$, and $u_{ij,k}^{\tau}$:

$$\begin{aligned} &u_{ij,k}^{\tau} \le x_{ij}^{\tau}, \\ &u_{ij,k}^{\tau} \le y_{j,k}, \\ &u_{ij,k}^{\tau} \ge x_{ij}^{\tau} + y_{j,k} - 1. \end{aligned} \tag{16}$$

Consequently, the objective function can be expressed as follows:

$$\begin{aligned} z_k(x_{ij}^{\tau}, y_{j,k}) = &\sum_{j\in J} \mathrm{f}_{j,k} y_{j,k} + \left(\sum_{i\in I}\sum_{j\in J}\sum_{\tau\in T}\sum_{k'\in K, k'\ne k} \mathrm{c}_{\mathrm{c},j}^{\tau} \varepsilon_{ij} u_{ij,k'}^{\tau} + \sum_{i\in I}\sum_{j\in J}\sum_{\tau\in T} \mathrm{c}_{\mathrm{o},j}^{\tau} \varepsilon_{ij} u_{ij,k}^{\tau} \right) \\ &+ \sum_{i\in I_k}\sum_{j\in J}\sum_{\tau\in T} w_{ij} \underline{x_{ij}^{\tau}} + \sum_{i\in I_k} \lambda_i \left(t_i^{\mathrm{s}} - e_i \right). \end{aligned} \tag{17}$$

To summarize, the collaborative scheduling problem is modeled by Eqs. (1) and (3)–(17), which is inherently a **bi-objective integer linear programming model**. The model incorporates binary decision variables x_{ij}^{τ} and $y_{j,k}$, as well as auxiliary binary variables $\underline{x_{ij}^{\tau}}$, $\overline{x_{ij}^{\tau}}$ and $u_{ij,k}^{\tau}$ alongside auxiliary integer variables t_i^{s} and t_i^{f}. By minimizing the costs for each company, the two objective functions address the inherent conflicts in collaborative scheduling. The model also incorporates key constraints, including charging continuity, location, time, demand, and capacity constraints, as well as charger capacity and rental constraints, ensuring the practicality and feasibility of the scheduling framework.

4. Solution methods

This section presents the methods developed to support decision-making in the proposed framework. Instead of exhaustively enumerating all efficient solutions, the approach focuses on generating a representative set of solutions that can effectively guide the final decision. To this end, the solution process consists of two parts. The first part develops a criterion-space search method, referred to as B3M, to efficiently construct a representative efficient frontier. The second part applies cooperative bargaining techniques to select a single agreement solution from this frontier that reflects fairness and mutual acceptability between participating companies. In this study, we focus on the bi-objective (two-operator) case because the B3M relies on geometric properties specific to two-dimensional non-dominated frontiers. Extending exact frontier identification to three or more objectives generally requires fundamentally different algorithmic frameworks.

The B3M represents a significant enhancement of the balanced box method, addressing its limitations in handling computational efficiency and solution representativeness. Unlike the original balanced box method, which focuses solely on accurately delineating the exact efficient frontier, the B3M introduces a novel mechanism to generate an efficient frontier. This mechanism strategically filters out closely positioned solutions, thereby reducing computational complexity while preserving the diversity and representativeness of the solution set. Once the efficient frontier has been established, cooperative bargaining methods are implemented to select the final optimal solution, ensuring a balanced and collaborative outcome. By integrating these innovations, the B3M not only maintains the strengths of the original balanced box method but also significantly enhances its applicability to complex bi-objective optimization problems. The notation used throughout this section is summarized in Appendix A.

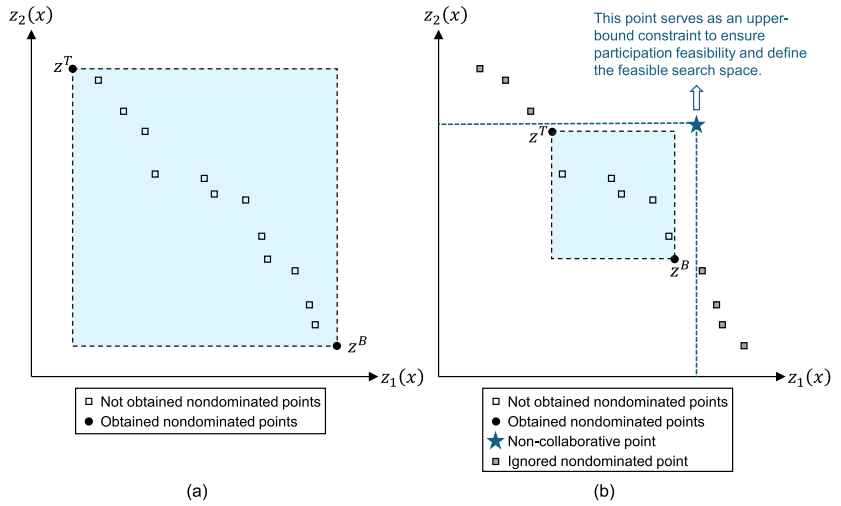

Fig. 2. Balanced box method: (a) unbounded search space, (b) incorporating non-collaborative point.

4.1. *Balanced bounding box methods*

The balanced bounding box method (B3Ms) is inspired by the **balanced box method**, which has been recognized for its ability to efficiently identify the exact efficient frontier compared to other criterion space exploration techniques (Boland et al., 2015). The balanced box method systematically explores rectangles within the criterion space, with the flowchart and main steps provided in Appendix B. A detailed description of its procedure is available in Boland et al. (2015).

Definition 1 (Participation constraints in collaborative optimization)**.** A participation constraint ensures that a company's cost in a collaborative solution does not exceed its cost in a non-collaborative scenario. In this study, we introduce a threshold condition guaranteeing that every company benefits from collaboration compared to its independent operation. This constraint does not define the entire feasible solution space but serves as a necessary condition to exclude unreasonably unfavorable outcomes and ensure voluntary participation in the collaboration.

In the non-collaborative scenario, each company independently solves its own charging station rental and scheduling problem without coordination with the other company. The resulting solution, obtained by separate optimizations under the same system parameters but without shared decision variables, is used as the non-collaborative reference point in the proposed method.

4.1.1. *Incorporating participation constraints for collaboration*

To ensure efficiency in collaborative optimization problems, the **B3Ms** framework imposes participation constraints that restrict solutions where a company's cost would exceed its non-collaborative scenario. Specifically, we introduce a threshold constraint (Zhou et al., 2024), ensuring that each company's cost remains below a predefined benchmark derived from its independent operation. This benchmark, denoted as z^{Non}, serves as an upper bound for the objectives in collaboration and is formulated as:

$$z_k \leq z_k^{\text{Non}}, \forall k \in K. \tag{18}$$

This condition effectively constrains the search space, ensuring that only solutions aligning with collaborative goals are considered. As illustrated in Fig. 2, the initial search space is constrained by the participation constraints, which use the non-collaborative point as a reference. This ensures that only solutions where both companies benefit from collaboration are considered feasible. Rather than directly influencing the determination of the efficient frontier, these constraints delineate the feasible region for collaboration, excluding solutions that result in worse outcomes than the non-collaborative scenario to guarantee voluntary participation.

Given these constraints, the initial and final points of the efficient frontier (z^T and z^B) are determined by solving the following two equations:

$$z^T := \underset{x \in \mathcal{X}}{\text{lexmin}} \left\{ z_1(x), z_2(x) : z(x) \in R((0, z_1^{\text{Non}}), (0, z_2^{\text{Non}})) \right\} \tag{19}$$

and

$$z^B := \underset{x \in \mathcal{X}}{\text{lexmin}} \left\{ z_2(x), z_1(x) : z(x) \in R((0, z_1^{\text{Non}}), (0, z_2^{\text{Non}})) \right\}, \tag{20}$$

This entails that the objectives are minimized sequentially according to a predefined priority. respectively. In Eqs. (19) and (20), "lexmin" denotes a lexicographic optimization approach, wherein the objectives are minimized in a sequential manner. This entails that the objectives are minimized sequentially according to a predefined priority. Eq. (19) initially minimizes $z_1(x)$, subsequently

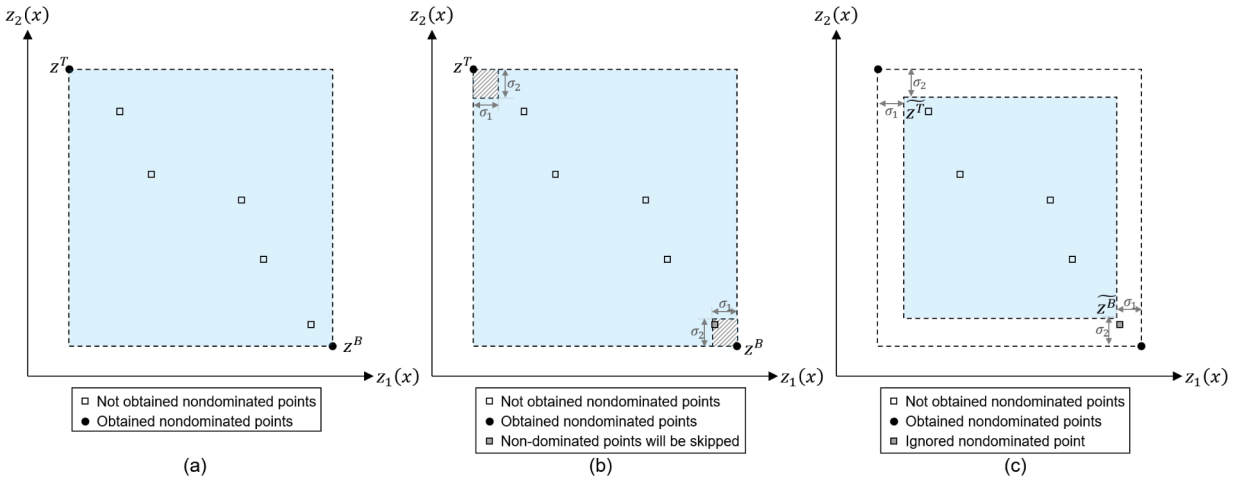

Fig. 3. Balanced box methods (a) original, (b) B3M with $z^n \approx \mathcal{Z}^e$, (c) B3M with $z^n \sim \mathcal{Z}^e$.

minimizing $z_2(x)$ while treating the objective values of $z_1(x)$ as constraints. Similarly, Eq. (20) applies the fundamental principle. Note that each point requires two processing stages to obtain the complete solution.

It should be noted that in defining the initial search space, we incorporate participation constraints using the non-collaborative point as a reference rather than considering an unbounded space. This ensures that only solutions where all companies benefit from collaboration are retained, effectively filtering out infeasible solutions and significantly reducing computational time.

Based on the identified initial and final points of the efficient frontier, the initial rectangle is defined as $R(z^T, z^B)$. The process of exploring rectangles involves dividing a rectangle into two smaller regions: the upper and lower rectangles (R^T and R^B). These two rectangles are defined by the points z^T, z^t, z^b, and z^B, where $z^t = (z_1^B, (z_2^T + z_2^B)/2)$ and $z^b = (z_1^T, (z_2^T + z_2^B)/2)$. The original rectangle is divided horizontally along the $z_2(x)$ axis and then removed from the rectangle set. New non-dominated points are identified by solving lexicographic optimization problems within these regions, and new rectangles are added to update the rectangle set. Smaller rectangles created during the process are handled in the same way. This iterative process continues until the rectangle set is empty, at which point all non-dominated points are identified. Further details of the two B3Ms will be introduced later.

4.1.2. The fundamental concept of B3Ms

The fundamental concept underlying the B3Ms is the exclusion of solutions that are close to one another. This ensures that the frontier generation process works efficiently and also speeds up computational time. The B3Ms optimize the solution framework to identify partial non-dominated solutions that are capable of representing the entire solution set. By excluding close solutions, the method avoids potential challenges in decision-making, such as difficulties in distinguishing among nearly equivalent solutions. Furthermore, it robustly discovers and represents the diversity that exists within the solution space, ensuring stable performance even when confronted with complex structures. Accordingly, the B3M generates a reduced solution set $\tilde{\mathcal{Z}}$, which is a subset of the original solution set $\mathcal{Z}$ with preserved diversity.

Definition 2 (Relative closeness). We define a new solution z^n as being very close if it closely resembles an existing solution z^e, where z^e belongs to the set $\mathcal{Z}^e$. The degree of closeness is characterized by two distinct scenarios:

- ***Definition 2.1: Strict closeness*** *$z^n \approx \mathcal{Z}^e$ is defined if for all $z^e \in \mathcal{Z}^e$, the conditions $z_1^e - \sigma_1 \le z_1^n \le z_1^e + \sigma_1$ and $z_2^e - \sigma_2 \le z_2^n \le z_2^e + \sigma_2$ are simultaneously satisfied.*
- ***Definition 2.2: Relaxed closeness*** *$z^n \sim \mathcal{Z}^e$ is defined if for all $z^e \in \mathcal{Z}^e$, either the condition $z_1^e - \sigma_1 \le z_1^n \le z_1^e + \sigma_1$ or $z_2^e - \sigma_2 \le z_2^n \le z_2^e + \sigma_2$ is met.*

where σ_1 and σ_2 are tolerance margins for objectives 1 and 2, indicating the allowable range for closeness.

Two B3Ms were developed, each grounded in the concept of a respective closeness. The first, designated B3M1, is defined as $z^n \approx \mathcal{Z}^e$, while the second, designated B3M2, is defined as $z^n \sim \mathcal{Z}^e$. Fig. 3 illustrates all the balanced box methods, including the original balanced box method, B3M1, and B3M2. The search area of interest is shown in blue. This is after the initial and final points of the efficient frontier have been determined.

As shown in Fig. 3, the search area of the B3M1 excludes only the small rectangles in the upper-left and lower-right corners. The B3M2, on the other hand, restricts the search area to the inner rectangle only.

4.1.3. Balanced bounding box method 1

The Balanced Bounding Box Method 1 (B3M1) is based on the strict closeness condition defined in Definition 2.1, where a new solution, denoted z^n, is deemed to be sufficiently close to the existing solution set, denoted $\mathcal{Z}^e$, to determine whether it is sufficiently close. This approach

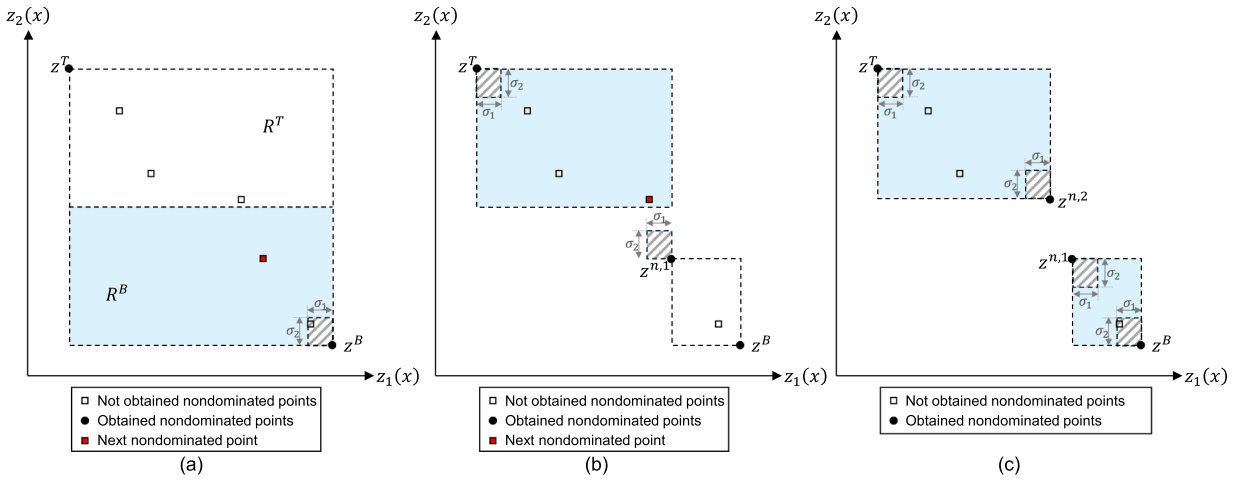

Fig. 4. B3M1, $z^n \approx \mathcal{Z}^e$, (a) investigating R^B, (b) investigating R^T, (c) new rectangles.

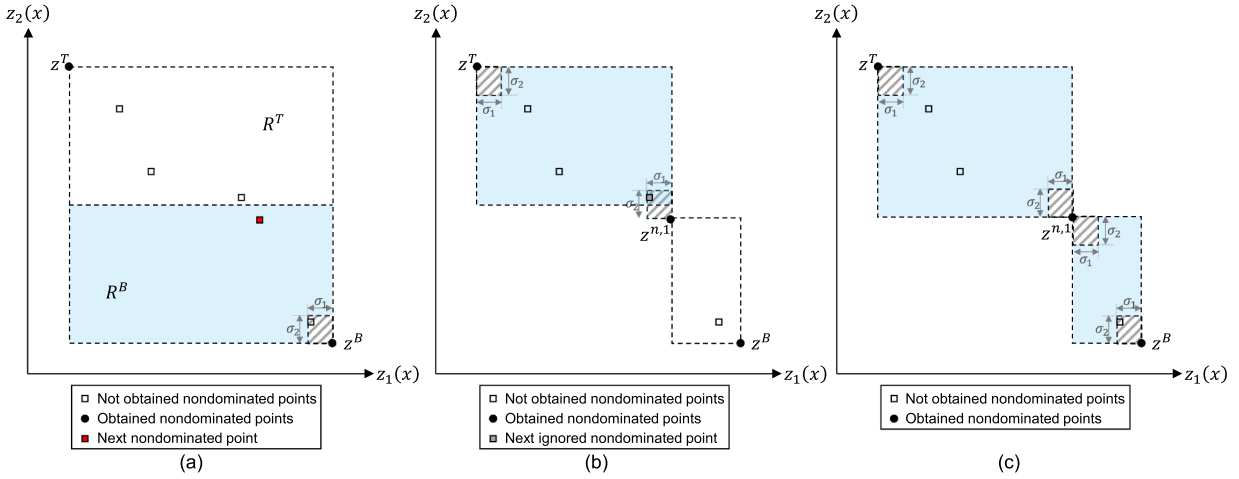

Fig. 5. B3M1, $z^n \approx \mathcal{Z}^e$, **special scenario**, (a) investigating R^B, (b) investigating R^T, (c) new rectangles.

ignores two minor rectangular regions (the upper-left and lower-right corners) to streamline the search space. Once a non-dominated point has been identified, the method evaluates its closeness according to the strict conditions of Definition 2.1 and terminates the search in the current region if the conditions are met.

As shown in Fig. 3 (b), for each rectangle, only the small rectangles in the upper-left and lower-right corners, marked by hatched areas, are ignored. The detailed steps of the method, including the comparison process in the lower and upper rectangles, are illustrated in Figs. 4 and 5.

Fig. 4 (a) illustrates the search in the lower rectangle R^B, where the new solution is compared to the lower-right point. If the new solution lies outside the hatched area, it is recorded as a new non-dominated point; otherwise, no new rectangles are identified. Fig. 4 (b) shows the search in the upper rectangle R^T, where the new solution is compared with the upper-left point and the newly obtained solution $z^{n,1}$ from the lower rectangle, or the lower-right point if $z^{n,1}$ does not exist. As illustrated in Fig. 4 (b), since the new solution is not close to either z^T or $z^{n,1}$, it is recorded as a new non-dominated point. After searching the lower and upper rectangles, two new non-dominated points are obtained, similar to the original balanced box method. Consequently, two new rectangles are identified, as shown in Fig. 4 (c).

Nevertheless, there is a special situation where the solution found in the upper rectangle is close to the solution found in the lower rectangle, as illustrated in Fig. 5 (b). The new solution is close to $z^{n,1}$ and should therefore be ignored. The non-dominated points obtained in this case are z^T, z^B, and $z^{n,1}$, resulting in the two new rectangles depicted in Fig. 5 (c). Notably, the search area in Fig. 5 (c) is larger compared to the scenario where two new non-dominated points are identified, as shown in Fig. 4 (c). In this situation, the rectangle $R(z^T, z^{n,2})$ and the rectangle $R(z^{n,1}, z^B)$ in Fig. 4 (c) can also represent the new search area of the original balanced box method. Consequently, this special case results in a larger search area due to the exclusion of some solutions, which we speculate may lead to an increase in computational time.

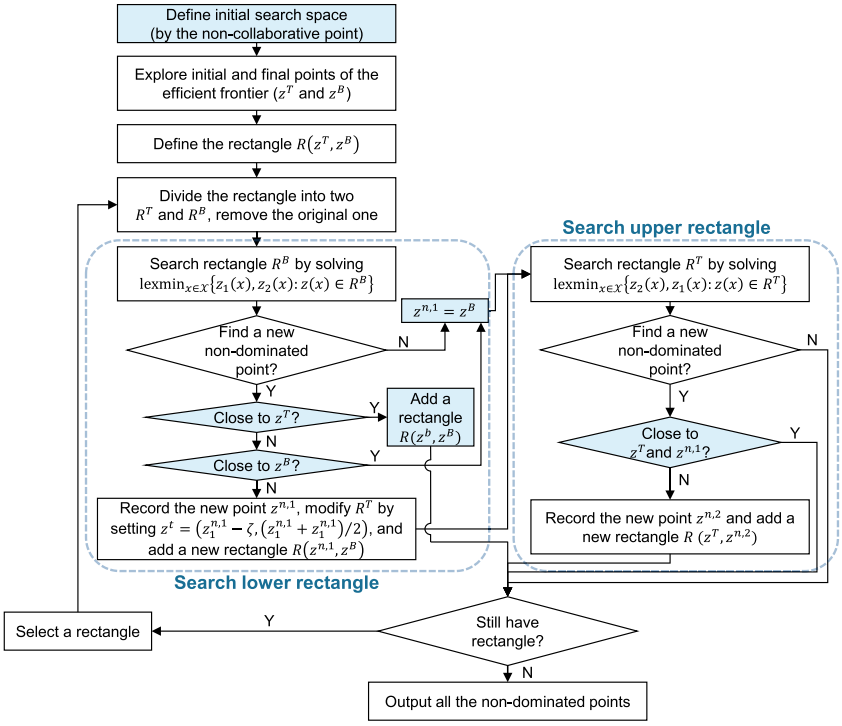

Fig. 6. The flowchart of B3M1.

The flowchart in Fig. 6 illustrates the detailed procedures for B3M1. The steps that have been revised or newly introduced are highlighted in blue, providing a clear distinction between the original and modified processes. As shown, the most significant modification is the addition of judgment steps for evaluating closeness based on strict conditions.

4.1.4. Balanced bounding box method 2

The Balanced Bounding Box Method 2 (B3M2) is based on the relaxed closeness condition defined in Definition 2.2, where solutions satisfying the condition $z^n \sim \mathcal{Z}^e$ are disregarded. Similar to the original balanced box method, this method requires the definition of rectangles. However, unlike the original method, where the rectangle is defined by z^T and z^B (as shown in Fig. 3 (a)), the rectangle in this method is defined by the relaxed boundaries $\tilde{z^T} = (z_1^T + \sigma_1, z_2^T - \sigma_2)$ and $\tilde{z^B} = (z_1^B - \sigma_1, z_2^B + \sigma_2)$, as shown in Fig. 3 (c). The method explores the middle region between $\tilde{z^T}$ and $\tilde{z^B}$, ignoring solutions that satisfy the relaxed closeness condition.

The procedures of the B3M2, based on the relaxed closeness condition, are depicted in Fig. 7.

As depicted in Fig. 7, the inner blue rectangle is smaller than the outer transparent rectangle, indicating a considerable reduction of the search space at each step in the B3M compared to the original one. The lower rectangle $\tilde{R^B}$ is defined by the points $\tilde{z^b}$ and $\tilde{z^B}$, where $\tilde{z^b}$ is $(\tilde{z_1^T}, (\tilde{z_2^T} + \tilde{z_2^B})/2)$. Upon searching the lower rectangle $\tilde{R^B}$, the red point in Fig. 7 (a) is obtained, denoted as $z^{n,1}$. Note that if a new non-dominated point $z^{n,1}$ is discovered in the lower rectangle, the upper rectangle $\tilde{R^T}$ should be adjusted in relation to the newly obtained point. The upper rectangle $\tilde{R^T}(\tilde{z^T}, \tilde{z^t})$ should be modified by setting $\tilde{z^t} = \left(z_1^{n,1} - \sigma_1, \max\left(z_2^{n,1} + \sigma_2, (\tilde{z_2^T} + \tilde{z_2^B})/2\right)\right)$. As illustrated in Fig. 7 (b), if $z_2^{n,1} + \sigma_2 \le (\tilde{z_2^T} + \tilde{z_2^B})/2$, then the lower bound for objective 2 is $(\tilde{z_2^T} + \tilde{z_2^B})/2$. The search area in the upper rectangle is represented by the blue area, with the red point indicating the newly obtained solution. Furthermore, the gray point in the lower rectangle of Fig. 7 (b) is excluded due to its proximity to the non-dominated point z^B. Similarly, in Fig. 7 (c), the gray point in the middle is excluded because of its closeness to the non-dominated point $z^{n,1}$. This results in the identification of two new rectangles, shown as the blue areas in Fig. 7 (c). In this case, the B3M yields two fewer non-dominated points compared to the original method. The detailed B3M2 procedure is shown in Appendix B (Fig. B2), where purple highlights denote revised or new steps.

Definition 3 (Tolerance range)**.** The term "tolerance range," as represented by the variable ϵ, expressed as a percentage, is that which is required to ensure consistency in the scaling of two objectives. The optimal solutions for these objectives are represented by z_1^T and z_2^B, respectively. In consequence, the tolerance margins for objectives 1 and 2 are defined as follows: $\sigma_1 = \epsilon z_1^T$ and $\sigma_2 = \epsilon z_2^B$. These margins serve to establish the permissible deviation from the optimal solutions, thereby quantifying the degree of acceptance within the specified tolerance range.

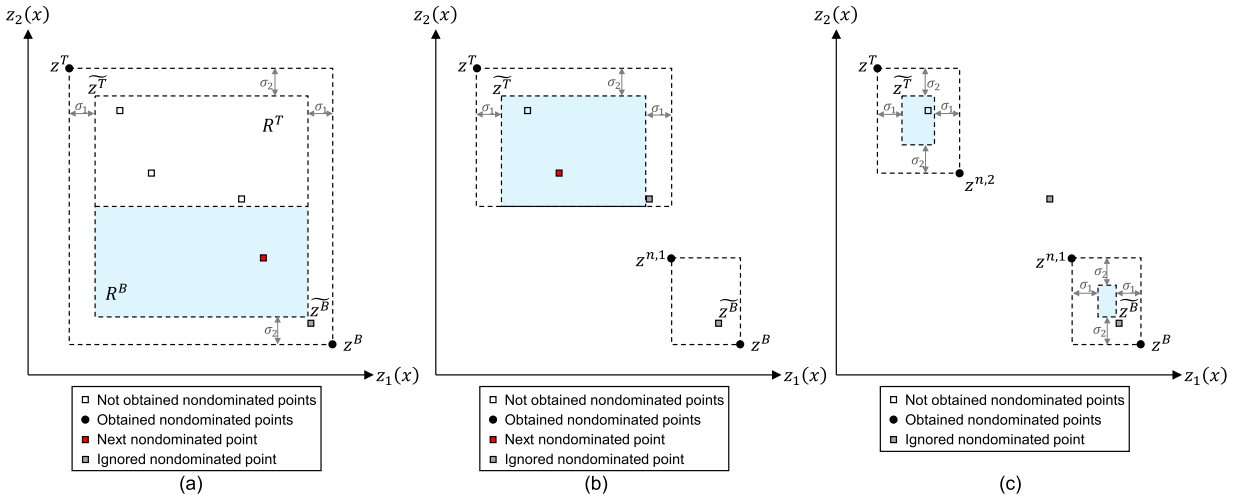

Fig. 7. B3M2, $z^n \sim \mathcal{Z}^e$, (a) investigating R^B, (b) investigating R^T, (c) new rectangles.

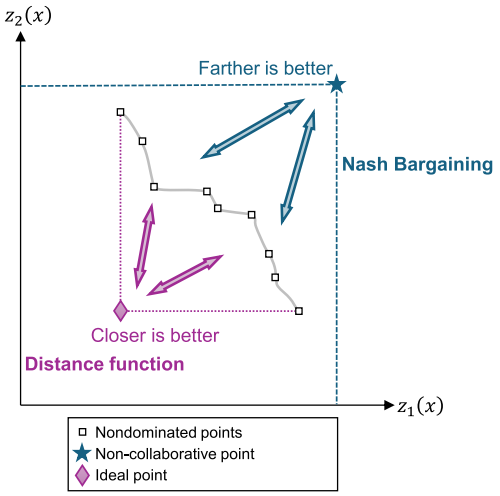

Fig. 8. Illustration of cooperative bargaining.

4.2. Cooperative bargaining

The solution approaches proposed in Section 4.1 can derive an efficient frontier. This section is dedicated to the identification of a final solution from the obtained frontier. Given that the two objectives in the bi-objective optimization are neither fully aligned nor entirely opposed, it is possible for players to collaborate in order to reach a mutually agreeable solution. The process is facilitated by the introduction of cooperative bargaining. We use the Nash bargaining solution, which provides a unique outcome in such games, to ensure an enforceable agreement based on specific axioms (Nash, 1953).

Before proceeding with a detailed examination of the cooperative bargaining techniques, it is crucial to underscore the fundamental objective of such bargaining: to identify a final solution that represents the greatest distance from the non-collaborative point while simultaneously approaching the ideal point. The aforementioned concepts are illustrated in Fig. 8 and correspond to the two bargaining methods, namely generalized Nash bargaining and the distance function.

4.2.1. Generalized Nash bargaining

The initial step is to compare each solution on the frontier with the non-collaborative solution. This allows us to identify the final agreement point. The optimal agreement point is the one farthest from the non-collaborative solution. In scenarios where the two players possess unequal bargaining power, let π and $1-\pi$ denote the relative bargaining strengths of Player 1 and Player 2,

respectively. Under these conditions, the Nash bargaining solution is given by the following formulation:

$$s^* = \underset{(z_1,z_2)\in\mathcal{Z}}{\operatorname{argmax}} (\bar{z}_1 - z_1)^{\pi}(\bar{z}_2 - z_2)^{1-\pi}, \tag{21}$$

where $\bar{z}_1$ and $\bar{z}_2$ denote the costs incurred by both companies in the non-cooperative scenario, indicating the maximum cost that they would be willing to accept for such collaboration. In the symmetric case, the exponents are both equal to 1/2 and sum to 1, thereby ensuring normalization. These exponents represent the bargaining power of each player. As π increases, player 1 receives a larger share in equilibrium, and vice versa.

4.2.2. Distance function

An alternative method for identifying the final agreement point is to evaluate the distance between frontier solutions and the ideal point. The optimal agreement solution is the one closest to the ideal point, measured by a distance function:

$$D_\alpha(z_1, z_2) = \left[\left(\frac{z_1 - \underline{z}_1}{\bar{z}_1 - \underline{z}_1}\right)^{\alpha} + \left(\frac{z_2 - \underline{z}_2}{\bar{z}_2 - \underline{z}_2}\right)^{\alpha}\right]^{1/\alpha}, \tag{22}$$

where $\underline{z}_k$ and $\bar{z}_k$ denote the minimal and maximal values of each objective. The parameter α controls the sensitivity of distance measurement. The optimal point s^* on the frontier is then:

$$s^* = \underset{(z_1,z_2)\in\mathcal{Z}}{\operatorname{argmin}} \; D_\alpha\big(z_1, z_2\big). \tag{23}$$

For $\alpha = 1$, the metric becomes the Manhattan norm, and for $\alpha = 2$, the Euclidean norm. The α-norm thus offers a unified way to represent fairness-efficiency trade-offs, with detailed mathematical properties summarized in Appendix C.

Although specific parameter values of π and α would theoretically determine a unique bargaining outcome, these parameters are typically unknown prior to negotiation. In this context, the representative non-dominated frontier obtained from the preceding section provides a transparent negotiation domain that bridges theoretical bargaining constructs with practical decision making. Within this domain, companies can jointly explore efficiency-fairness trade-offs and identify suitable settings of π or α to determine the final agreement point, thereby facilitating a mutually acceptable cooperative solution.

5. Case study

In this section, we demonstrate the proposed model and solution methods using case studies based on real-world scenarios.

5.1. Scenario setting

The case studies utilize real-world data on locations, charging rates, and pricing from charging stations operated by Göteborg Energi, the largest energy provider in Gothenburg, Sweden. In this study, Göteborg Energi acts as a third-party provider, while the collaboration takes place between two fleet operators. The two-operator setting already captures coordination trade-offs and fairness considerations that arise in collaborative charging. The dataset includes precise station locations, along with details on charging power and pricing. Fig. 9 illustrates the charging station locations and the randomly distributed EVs to represent spatially heterogeneous demand within a 20 km × 20 km service area, where the framed region represents the service boundary. The two fleet operators are represented in green and orange, respectively, whereas the charging stations available for rent are shown in grey. The distance traveled by vehicles to reach these charging stations is calculated using a real-world map and leveraging the OpenRouteService (ORS) API (openrouteservice, 2024).

Given the inherent uncertainty in charging demand, we simulate charging requests from EVs distributed across the service area. The hourly electricity prices are obtained from Nord Pool's official market data (Nord Pool, 2024), and the public charging fee represents the prices charged by Göteborg Energi's charging stations. Fig. 10 illustrates an example of fluctuating electricity prices and public charging fees over a 24-hour period, revealing the temporal price trends at different times of the day.

Two fleet operators collaborate within the system, denoted as K. Each fleet operator k manages a group of EVs, I_k, while Göteborg Energi provides a set of chargers, J. The service period under consideration spans one day, which is divided into 24 one-hour intervals (T) to allow for precise time-specific scheduling adjustments. Each charging station incurs a fixed daily rental fee, f_j^k, which is calculated on a per-day basis. This reflects a flexible rental strategy that is ideally suited to accommodate fluctuating demand. The fixed daily rental fee is set at 1500 SEK, based on the public charging fee and roughly equivalent to the cost of using a public charging station for 7 hours. To maintain general applicability, this study considers only charging stations from Göteborg Energi with a maximum charging rate of 50 kW, which corresponds to the previously defined charging rate ε_{ij}. In scenarios with more stable demand, alternative business models (such as subscription-based models, long-term leasing agreements, or even the construction of new facilities) could be considered. When a company rents a charging station, it is required to pay the electricity fee, denoted as $c_{\mathrm{e,o}}^{j,\tau}$. For collaborative EVs, a discount factor β of 0.5 is applied, meaning that a collaborating company pays half of the public charging fee when utilizing charging stations rented by others. This corresponds to the previously defined unit energy fee for collaborative EVs, $c_{\mathrm{e,c}}^{j,\tau}$. Additionally, the cost of waiting for charging, represented by λ_i, is estimated at 300 SEK per hour. The energy cost for EV i traveling to charger j, denoted by w_{ij}, is calculated based on the unit energy consumption cost of 6 SEK per kilometer.

In order to assess the performance at different scales, three cases with varying numbers of EVs were examined. In Case #1, there are 20 EVs, in Case #2, there are 30 EVs, and in Case #3, there are 40 EVs.

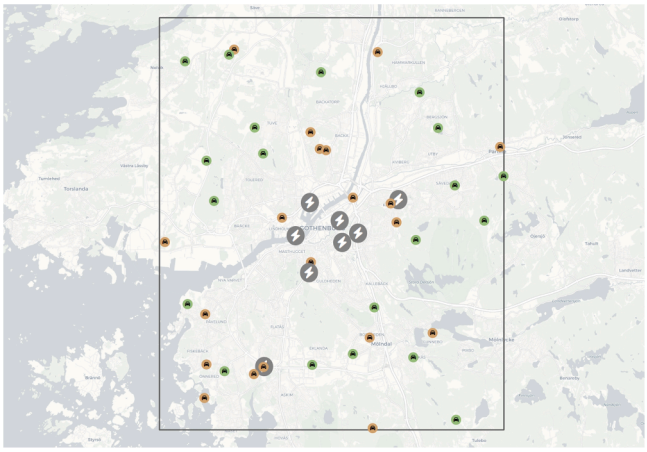

Fig. 9. Geographical distribution of charging stations and EVs.

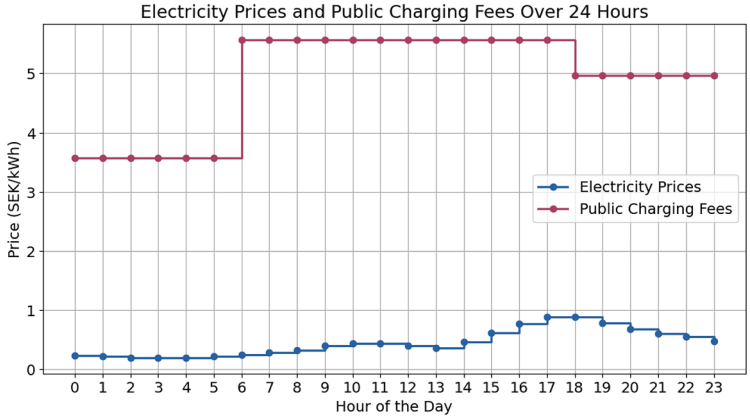

Fig. 10. Hourly fluctuations in electricity prices vs. public charging fees.

5.2. Computational performance

This section presents the computational performance of the developed B3Ms on a set of test cases, considering various distributions of EVs and chargers, and including comparisons with the Balanced Box Method, ϵ-constraint, and Tchebycheff approaches. The EV locations follow two spatial distributions: uniform and clustered, while chargers are arranged using two distinct layouts: uniform and centralized (see Fig. 11). Each EV is assigned a time window within a 24-hour period, with the earliest start time randomly generated between hours 1 and 20. The time window length is fixed at 4 hours, and each hour represents one time interval.

To distinguish between different test cases, we adopt the naming convention DistEV-DistChar-NumEV-NumCharger, where DistEV refers to the EV distribution (uniform or clustered), DistChar refers to the charger layout (uniform or centralized), and NumEV and NumCharger indicate the number of EVs and chargers, respectively. For example, UEV-UChar-50-10 represents a case where EVs are uniformly distributed, chargers follow a uniform layout, and there are 50 EVs and 10 chargers.

We evaluate the performance of B3M1 and B3M2 compared to the original balanced box method, ϵ-constraint, and Tchebycheff approaches. The tolerance range ϵ is set to 3%. Key performance metrics include the number of non-dominated points (NDP), computational time (CPU), solution gap percentage (Gap), and computational time savings (CTS). The Gap metric quantifies the quality loss of B3M-generated solutions compared to the original method. For each ignored solution (i.e., one not retained by B3M), we compute the Euclidean distance in the objective space to all retained solutions, based on their objective values. The smallest of these distances is recorded as the individual gap. The overall gap is then defined as the average of these individual gaps across all ignored solutions, providing a quantitative measure of the quality loss introduced by filtering out nearby solutions. CTS is calculated as the percentage reduction in CPU time compared to the original method.

Table 2 presents the computational results in terms of the number of NDP and CPU time. The proposed B3M variants consistently achieve shorter solution times than Balanced Box while maintaining comparable or higher coverage than ϵ-constraint and Tchebycheff. The comparative experiments were conducted under a fixed evaluation setting, where the weighting factor in the Tchebycheff method

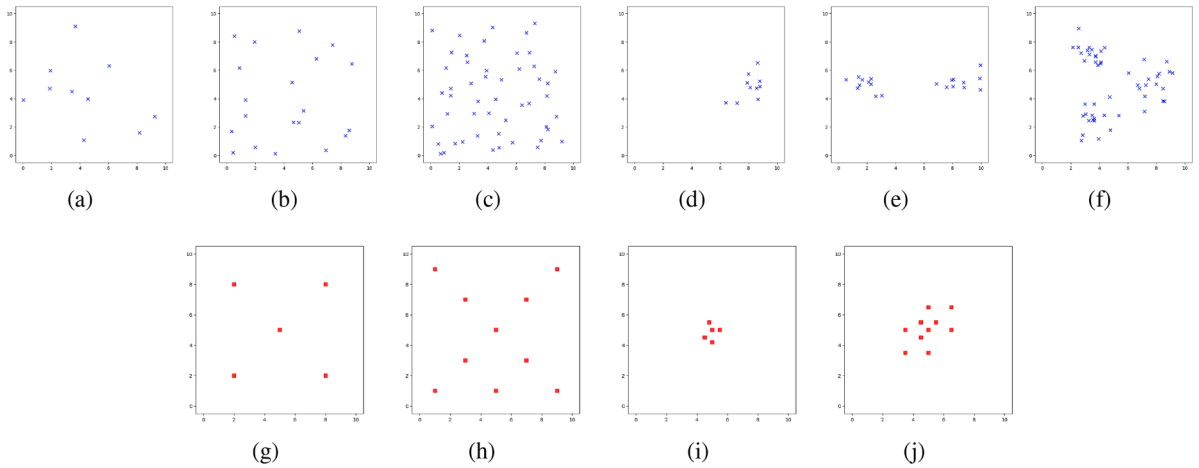

Fig. 11. Distribution of EVs and chargers in test cases. Subfigures (a)-(f) show electric vehicle (EV) spatial distributions with different fleet sizes (10, 20, 50) under uniform and clustered configurations. Subfigures (g)-(j) show charger layouts with two configurations (uniform and centralized) and varying charger counts (5 or 10).

Table 2
Computational results: NDP and CPU for all methods.

	ϵ-constraint		Tchebycheff		Balanced box		B3M1		B3M2	
Test cases	NDP	CPU	NDP	CPU	NDP	CPU	NDP	CPU	NDP	CPU
UEV-UChar-10-5	7	1407.6	7	1423.6	7	1314.6	5	1327.6	3	567.6
UEV-UChar-10-10	5	2803.4	6/8	2874.4	12	4492.7	5	2433.5	3	1083.4
UEV-UChar-20-5	4	2828.0	3/4	2886.2	4	1513.7	3	1512.4	2	756.4
UEV-UChar-20-10	5	5808.5	4/6	5884.7	7	5515.9	2	2037.0	2	1496.1
UEV-UChar-50-5	7/12	7504.0	12/18	7726.1	39	90049.2	5	19601.3	4	4164.3
UEV-UChar-50-10	6/7	16255.9	1/14	16894.2	32	147989.1	6	24876.4	4	9772.7
UEV-UChar-100-10	15/21	36592.1	14/20	36397.3	55	178027.6	6	53843.6	3	12383.6

Note: CPU time is measured in seconds (s). NDP values are expressed as On-front/Total solutions, with “On-front” denoting the number of solutions on the exact frontier. In cases where all solutions are on the frontier, only the total is reported.

varied by 0.05 in each iteration and the ϵ-constraint step was divided into 20 equal intervals. These fixed increments were chosen to ensure comparable solution resolution across methods while maintaining computational feasibility.

In most test cases shown in Table 2, the proposed B3M variants outperform the benchmark methods by achieving shorter computation times and comparable or higher coverage of the efficient frontier. Between the two variants, B3M1 provides a balanced performance, retaining more representative points at moderate computational cost, while B3M2 is consistently the fastest across all instances due to its stricter dominance filtering.

In contrast, the ϵ-constraint and Tchebycheff methods cannot guarantee global optimality under the adopted discretization settings, as they inherently depend on discretized step sizes and weighting parameters that determine the sampling resolution. Each frontier point is obtained from a single optimization under a fixed constraint or weight, without cross-objective re-optimization to verify true non-dominance. While their performance appears acceptable in a few small-scale cases, the solution quality deteriorates rapidly as problem size increases. The Balanced Box method, by comparison, remains globally exact but incurs substantially longer runtimes due to exhaustive exploration. Overall, these results demonstrate that the proposed B3Ms can markedly reduce computational effort while preserving solutions that lie on the exact efficient frontier, providing a reliable and computationally efficient approach for collaborative scheduling analysis.

Table 3 further reports the quality indicators (Gap and CTS) of proposed B3Ms in comparison with the Balanced Box method, demonstrating that B3M solutions are not only faster to compute but also achieve higher quality. As shown in Table 3, both B3M1 and B3M2 substantially reduce computational time while maintaining solution quality. B3M2 consistently achieves the highest CTS, especially in larger instances, with improvements frequently exceeding 60% and reaching up to 95.4%. B3M1 provides a balanced trade-off, offering notable time reductions while preserving accuracy comparable to the Balanced Box method. Both methods maintain comparable or lower non-dominated points, indicating their ability to remove closely positioned solutions without significantly reducing diversity, and the gap values remain within the 3% tolerance in almost all cases, confirming their global optimality as they lie on the exact efficient frontier, along with representative coverage. Further analysis across charger layouts and EV distribution settings reveals that spatial configuration strongly influences computational behavior. Centralized layouts concentrate chargers within compact regions, reducing CPU time but limiting flexibility, whereas uniform layouts enhance spatial diversity and produce more

Table 3
Solution quality comparison: Balanced Box vs. B3Ms.

	Balanced box	B3M1			B3M2		
Test cases	NDP	NDP	Gap	CTS	NDP	Gap	CTS
UEV-UChar-10-5	7	5	2.25%	-1.0%	3	3.18%	56.9%
UEV-UChar-10-10	12	5	1.30%	45.8%	3	2.23%	75.8%
UEV-UChar-20-5	4	3	0.84%	0.1%	2	2.80%	50.0%
UEV-UChar-20-10	7	2	2.03%	63.1%	2	2.03%	72.9%
UEV-UChar-50-5	39	5	1.34%	78.2%	4	1.68%	95.4%
UEV-UChar-50-10	32	6	1.39%	82.2%	4	1.91%	94.2%
UEV-CChar-10-5	7	3	0.55%	52.3%	3	0.55%	56.6%
UEV-CChar-10-10	10	3	1.52%	65.0%	3	1.52%	68.7%
UEV-CChar-20-5	5	2	0.65%	48.6%	2	0.65%	61.3%
UEV-CChar-20-10	12	2	0.95%	77.1%	2	0.95%	83.4%
UEV-CChar-50-5	13	2	0.37%	82.8%	2	0.37%	86.1%
UEV-CChar-50-10	14	4	1.05%	48.2%	2	2.94%	85.9%
CEV-UChar-10-5	4	3	0.36%	24.2%	3	0.36%	32.3%
CEV-UChar-10-10	4	3	0.46%	19.6%	3	0.46%	27.2%
CEV-UChar-20-5	11	3	1.40%	62.1%	3	1.50%	71.8%
CEV-UChar-20-10	10	2	1.17%	73.4%	2	1.17%	80.2%
CEV-UChar-50-5	21	4	1.77%	57.6%	3	2.47%	86.0%
CEV-UChar-50-10	33	5	1.48%	58.9%	4	2.16%	88.1%
CEV-CChar-10-5	6	3	0.37%	22.6%	3	0.37%	48.9%
CEV-CChar-10-10	4	3	0.47%	13.0%	3	0.47%	22.4%
CEV-CChar-20-5	4	2	0.19%	39.3%	2	0.19%	48.1%
CEV-CChar-20-10	3	2	0.48%	18.7%	2	0.48%	33.7%
CEV-CChar-50-5	5	2	0.26%	47.5%	2	0.26%	63.0%
CEV-CChar-50-10	21	4	1.81%	57.8%	3	2.64%	86.6%

non-dominated solutions at a higher computational cost. EV distribution has a less consistent influence. Overall, these results highlight the critical importance of charger placement and confirm the robustness of B3Ms across varied problem settings.

5.3. Results and analysis

This section presents detailed analyses of the optimization results to examine how the proposed methods perform under different parameter settings and decision scenarios. The results are discussed in terms of tolerance range effects, distribution of non-dominated points, sensitivity to behavioral and cost parameters, and the resulting cooperative scheduling outcomes.

5.3.1. Different tolerance range

This section presents an analysis of the impact of the tolerance range ϵ on the computational performance and solution sets. Specifically, we examine the three cases defined earlier (Case #1: 20 EVs, Case #2: 30 EVs, Case #3: 40 EVs). By varying the tolerance range ϵ, the relationship between CTS and NDP of three cases is illustrated in Fig. 12.

As illustrated in Fig. 12, an increase in the tolerance range is generally accompanied by a reduction in the number of non-dominated points and computational time. In all cases, the implementation of B3M2 in comparison to B3M1 has the potential to reduce computational time, although this may be at the cost of a reduction in the number of non-dominated points. The B3M2 has the potential to reduce computational time by over 50% compared to the original balanced box method when the tolerance range ϵ is set to at least 2%, and up to 95% when the range is increased further. Notably, once the tolerance range exceeds 6%, the resulting non-dominated solution sets obtained under different tolerance levels become highly similar, indicating an empirical saturation regime for the tested cases. In this regime, the efficient frontier is represented by only a few widely spaced points, and further increases in the tolerance primarily lead to a coarser representation of the frontier rather than additional insight into the underlying trade-offs. Accordingly, tolerance levels of 1%, 2%, and 5% are selected for detailed analysis, as they provide a more informative balance between solution resolution and computational efficiency.

Table 4 summarizes the outcomes of various methods, including the balanced box method and its two enhancements: B3M1 and B3M2. The summary provides the number of non-dominated points (NDP), the computational time (CPU), the predetermined tolerance range (ϵ), the gap between the B3M and the original balanced box method (Gap), and the computational time savings (CTS).

As can be seen in Table 4, the results align with the expectations regarding the design of the B3Ms. As defined in Section 4.1.2, the two B3Ms use different criteria for ignoring solutions based on the closeness measures $z^n \approx \mathcal{Z}^e$ and $z^n \sim \mathcal{Z}^e$. For B3M1, ignored solutions must have both objectives within the tolerance range ϵ. In contrast, for B3M2, only one objective has to be within the tolerance range ϵ. Several insights can be provided from the results. Firstly, it shows that the number of non-dominated points obtained from B3M1 is greater than that obtained from B3M2. Secondly, the gaps for B3M1 are generally smaller than the predetermined tolerance range ϵ, with exceptions observed in Case #3 (1.1% when $\epsilon = 1\%$). In contrast, the gaps for B3M2 frequently exceed the predetermined tolerance range, reflecting greater variability and reduced adherence to ϵ. For example, when $\epsilon = 5\%$, the gaps for B3M2 range from 4.3% (Case #3) to 7.0% (Case #1). Thirdly, the computational time for both B3Ms is significantly reduced with a

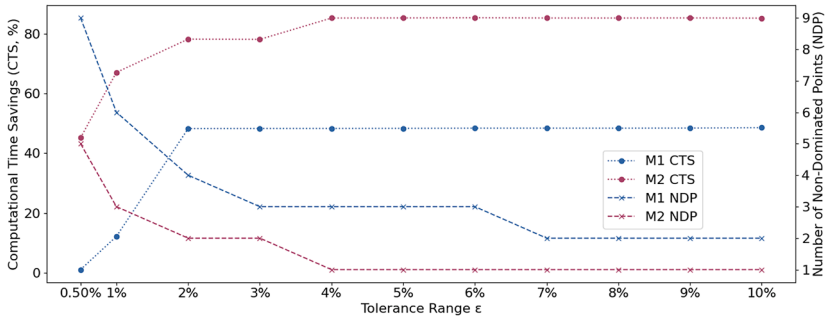

(a) Case #1

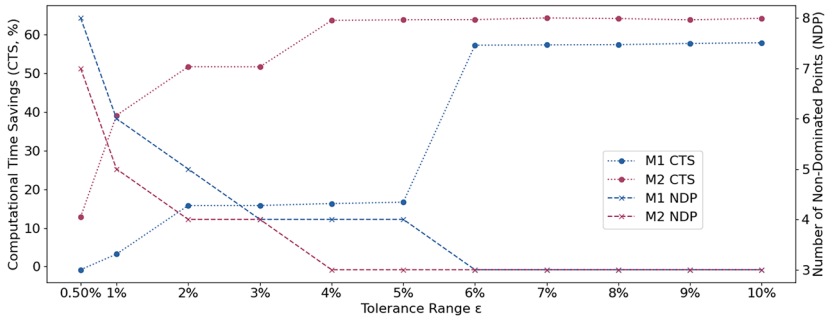

(b) Case #2

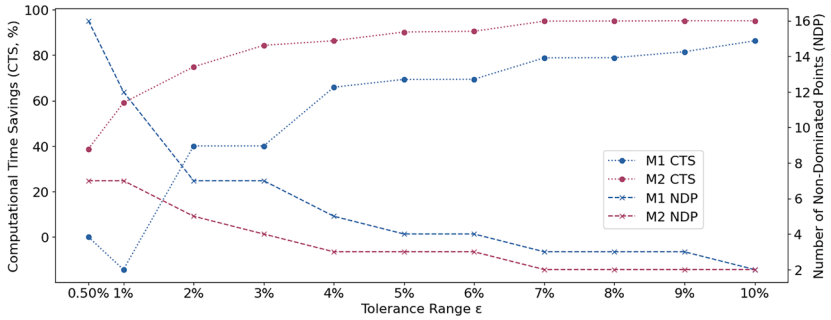

(c) Case #3

Fig. 12. Comparative analysis of results across various tolerance ranges ϵ.

Table 4
Results of different methods.

	Balanced box method		ϵ	B3M1				B3M2			
	NDP	CPU (s)		NDP	CPU (s)	Gap	CTS	NDP	CPU (s)	Gap	CTS
			1%	6	4778.2	0.9%	11.0%	3	1769.2	2.0%	67.0%
Case #1	9	5366.6	2%	4	2778.0	1.2%	48.2%	2	1173.5	3.8%	78.1%
			5%	3	2774.0	2.7%	48.3%	1	793.9	7.0%	85.2%
			1%	6	7261.7	1.0%	3.2%	5	4569.2	1.4%	39.1%
Case #2	8	7504.9	2%	5	6319.7	1.4%	15.8%	4	3627.1	3.4%	51.7%
			5%	4	6255.3	3.4%	16.7%	3	2715.9	5.2%	63.8%
			1%	12	57878.2	1.1%	-14.3%	7	20730.3	2.0%	59.1%
Case #3	17	50644.0	2%	7	30347.3	1.7%	40.1%	4	12714.6	2.5%	74.9%
			5%	4	15515.6	3.0%	69.4%	3	4964.2	4.3%	90.2%

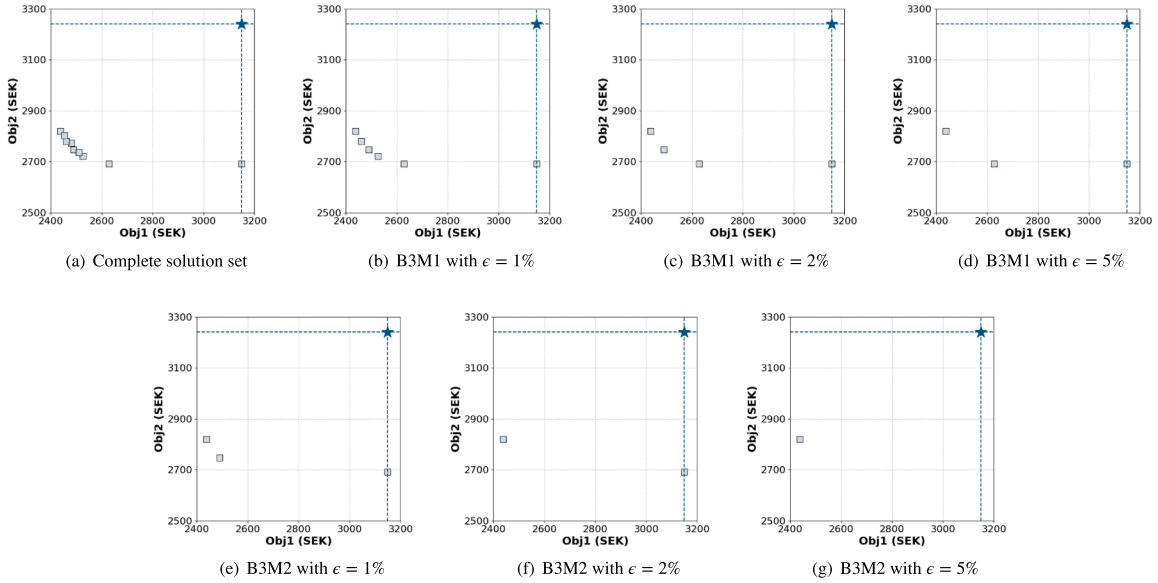

(a) Complete solution set (b) B3M1 with $\epsilon = 1\%$ (c) B3M1 with $\epsilon = 2\%$ (d) B3M1 with $\epsilon = 5\%$

(e) B3M2 with $\epsilon = 1\%$ (f) B3M2 with $\epsilon = 2\%$ (g) B3M2 with $\epsilon = 5\%$

Fig. 13. Non-dominated solutions of Case #1 with different methods.

larger tolerance range ϵ, with B3M2 demonstrating even more notable savings compared to B3M1. However, there is an exception in case #3 with $\epsilon = 1\%$: the computational time of B3M1 is longer than that of the balanced box method. This discrepancy arises because B3M1 disregards the solution by comparing it with the upper-left or lower-right points, which should be recorded as solutions. As a result, the search area is expanded in this particular instance.

5.3.2. *Distribution of non-dominated points*

The non-dominated solutions for the three cases are presented in Figs. 13–15. The figures illustrate the solutions obtained through the implementation of the original balanced box method and two B3Ms.

As observed in Fig. 13, the non-dominated solutions are primarily concentrated in the lower-left region in Case #1. With B3M1, the non-dominated solutions are distributed in a relatively uniform manner. In contrast, the use of B3M2 results in a reduction in the number of non-dominated points, particularly in scenarios where $\epsilon = 2\%$ and $\epsilon = 5\%$. This is due to the close proximity of the upper-left and lower-right points in terms of objective 2, limiting the diversity of reduced solutions. It can be concluded that if the variation in one of the objectives is insufficient, then B3M2 becomes ineffective. In such cases, B3M1 is recommended as a more suitable alternative.

In Fig. 14, the non-dominated points are mainly concentrated in the central region, forming a compact cluster of solutions. The non-dominated solutions are distributed relatively evenly among the two B3Ms. Given the similarity in the ranges of the two objectives, both methods yielded comparable results, with B3M2 producing a slight reduction in the number of non-dominated points.

As illustrated in Fig. 15, the number of non-dominated points is considerable, and no distinct clustering is evident. The distribution of non-dominated points is more uniform with B3M2, as illustrated in the two pairs of comparisons: Fig. 15 (c) vs. (f), and Fig. 15 (d) vs. (g). This is due to the fact that B3M2 is more aggressive than B3M1. In contrast to B3M1, which ignores a current solution only when the differences between both objectives and an existing solution fall within the tolerance range, B3M2 applies a stricter filtering rule. This is because B3M2 ignores a solution if either objective falls within the tolerance range. The advantage of B3M2 is that it facilitates a more uniform distribution of non-dominated points, thereby ensuring a greater degree of diversity and coverage across the objective space.

5.3.3. *Sensitivity analysis*

This section examines the effects of varying levels of value of time (VOT, λ) on the optimization process and the balance between competing objectives. Fig. 16 illustrates the comparative performance of collaborative and non-collaborative solutions at varying VOT levels, thereby demonstrating the influence on the optimization outcomes. The squares of different colors represent collaborative solutions; the dashed lines connect them to form a non-dominated frontier; the stars indicate the corresponding non-collaborative solutions.

As shown in Fig. 16 (a), an increase in VOT generally results in a more pronounced advantage of collaborative solutions over non-collaborative ones, particularly at higher VOT levels (e.g., $\lambda = 500$ SEK). At these levels, non-collaborative solutions deviate significantly from the frontier. This highlights the vital importance of collaboration in achieving superior outcomes under conditions of high VOT. As VOT increases, the trade-offs between objectives become more intricate, and the frontier becomes steeper, reflecting the growing challenge of decision-making. Notably, several points overlap across different VOT levels, indicating that certain solutions remain robust or near-optimal despite changes in VOT. These solutions could indicate regions of the solution space where trade-offs

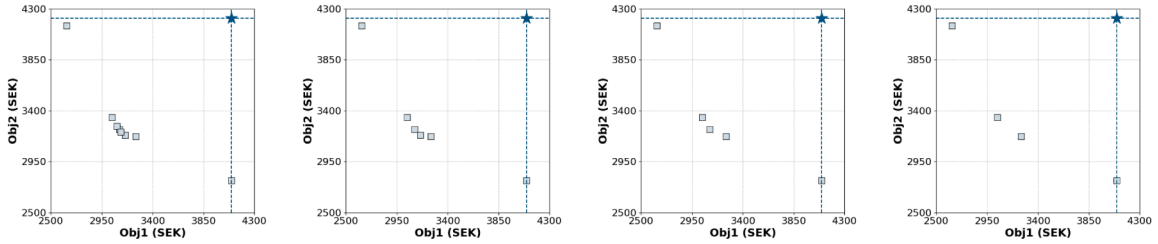

(a) All the solutions (b) B3M1 with $\epsilon = 1\%$ (c) B3M1 with $\epsilon = 2\%$ (d) B3M1 with $\epsilon = 5\%$

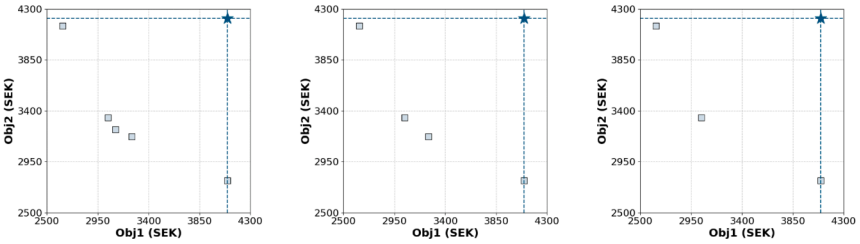

(e) B3M2 with $\epsilon = 1\%$ (f) B3M2 with $\epsilon = 2\%$ (g) B3M2 with $\epsilon = 5\%$

Fig. 14. Non-dominated solutions of Case #2 with different methods.

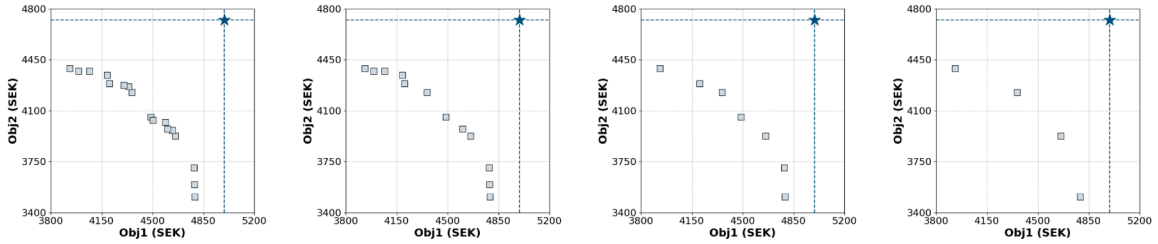

(a) All the solutions (b) B3M1 with $\epsilon = 1\%$ (c) B3M1 with $\epsilon = 2\%$ (d) B3M1 with $\epsilon = 5\%$

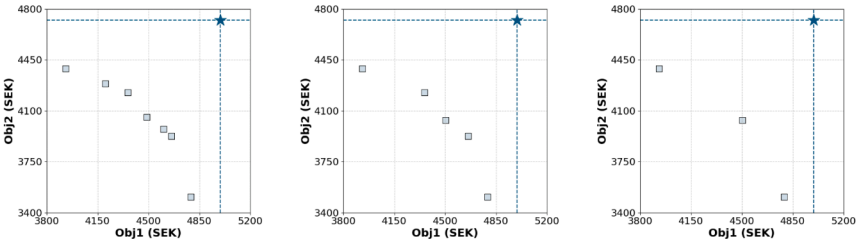

(e) B3M2 with $\epsilon = 1\%$ (f) B3M2 with $\epsilon = 2\%$ (g) B3M2 with $\epsilon = 5\%$

Fig. 15. Non-dominated solutions of Case #3 with different methods.

are less sensitive to VOT changes, supporting more stable decision-making strategies. Figs. 16 (b) and (c) compare the results of the two B3Ms at different VOT levels. With $\epsilon = 1\%$ in B3M1 (Fig. 16 (b)), the solutions are more precise, and the distance between collaborative and non-collaborative solutions is greater, especially at higher λ values. In contrast, B3M2 (Fig. 16 (c)) produces more dispersed solutions, reflecting its more aggressive nature. However, this can compromise precision, particularly at higher λ values. Due to page limitations, we present only the results of B3Ms with $\epsilon = 1\%$. As ϵ increases, the solution set becomes more dispersed, the efficient frontier flattens, and the advantage of collaboration diminishes. Higher ϵ values also reduce solution accuracy while shortening computation time, highlighting a trade-off between precision and computational efficiency.

In addition, the energy fees $c^{\tau}_{\mathrm{c},j}$ and $c^{\tau}_{\mathrm{o},j}$ are adjusted in parallel by a uniform scaling factor θ. The adjusted fees are then calculated as $c = c \times \theta$. This approach allows an investigation of the influence of proportional changes in both collaborative and own EV charging fees on the optimization results. Fig. 17 shows the impact of changes in unit energy cost (θ) on both collaborative and non-collaborative solutions.

In Fig. 17 (a), at lower unit energy costs (smaller θ), the distance between cooperative and non-collaborative solutions is greater, thereby emphasizing the necessity and advantages of collaboration. Conversely, as unit energy costs increase (larger θ), this distance

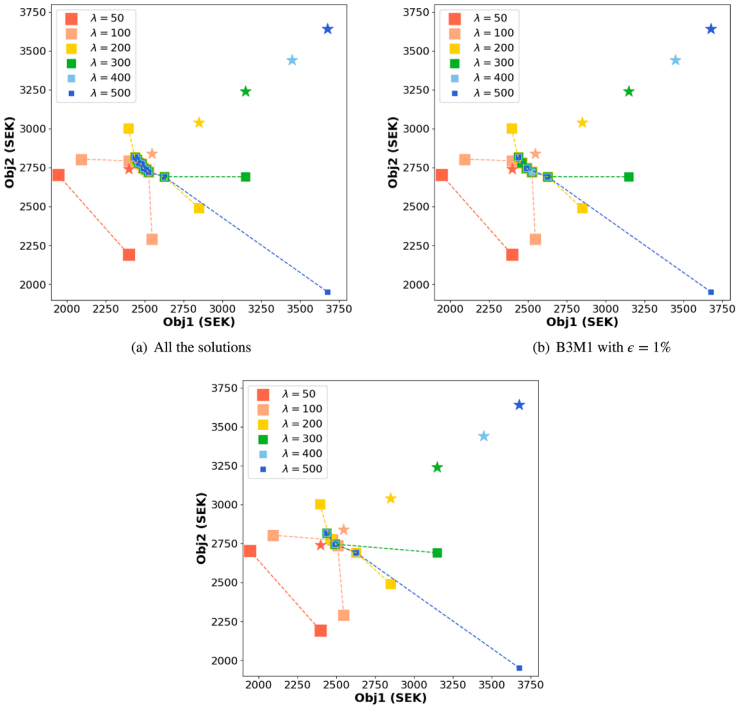

(a) All the solutions

(b) B3M1 with $\epsilon = 1\%$

(c) B3M2 with $\epsilon = 1\%$

Fig. 16. Impact of VOT levels (λ) on optimized results using B3Ms.

decreases, thereby diminishing the benefits and importance of collaboration. One potential explanation for this reduction in disparity is that rental costs for charging stations remain unchanged, which may prompt companies to prefer leasing stations on their own as energy costs rise. This may, in turn, result in a reduction in the necessity for collaboration. Furthermore, as the value of θ increases, the efficient frontier shortens, and the collaborative solutions become more concentrated. This indicates that higher energy costs limit the range of trade-offs between objectives, thereby reducing both the flexibility in optimization and the variety of available solutions. Figs. 17 (b) and (c) further extend the analysis by illustrating the impact of different scaling factors (θ) on the results of B3M1 and B3M2. A similar trend is observed in Fig. 16, with B3M2 continuing to demonstrate a more dispersed set of solutions across the θ values, reflecting its more aggressive nature. In contrast, B3M1 maintains a more concentrated set of solutions. This comparison serves to reinforce the trade-off between precision and solution flexibility across different B3Ms and error tolerances.

5.3.4. *Results of Nash bargaining*

The final solution is identified using the generalized Nash bargaining and the α-norm distance. The final solutions are illustrated in Figs. 18–20 for different parameters values. In each figure, square markers denote non-dominated points. Red squares mark the final agreements for specific parameter intervals, with the parameter values labeled next to each point. These red squares make explicit how the parameter ranges shape the trade-offs between the two objectives. Finally, a comparison of the final solutions based on the exact efficient frontier and the efficient frontier indicates no significant discrepancy between them, particularly when the distance function is utilized to identify the final agreement point.

As π increases, the agreement point moves smoothly along the representative frontier toward the upper-left region, reflecting a gradual redistribution of bargaining power between the two objectives. Lower π values favor the second objective, whereas higher values shift the compromise toward the first. The smooth transition of red markers in Figs. 18–20 indicates that moderate changes in π cause only limited movements of the agreement point, demonstrating the stability of the Nash bargaining outcomes. Such stability is desirable in practice, as it allows stakeholders to choose from a transparent, precomputed set of trade-offs without re-optimizing the problem.

Similar trends are observed for the α-norm formulation, which provides a geometric counterpart to the bargaining rule. When the norm parameter α is small (e.g., $\alpha = 1$), the two objectives receive nearly equal weighting, yielding balanced outcomes. Larger α values emphasize the largest normalized deviation and push the selected point toward more conservative regions of the frontier. In practice, α can be predefined as a small set of admissible values, allowing decision makers to select between balanced and robustness-oriented options during coordination.

Across all test cases, both formulations exhibit consistent and interpretable patterns. When the frontier is steep and the trade-off between objectives is strong, the Nash bargaining formulation achieves a slightly better balance between fairness and efficiency, whereas the α-norm approach tends to favor more conservative outcomes by limiting the worst deviation. In smoother frontiers where

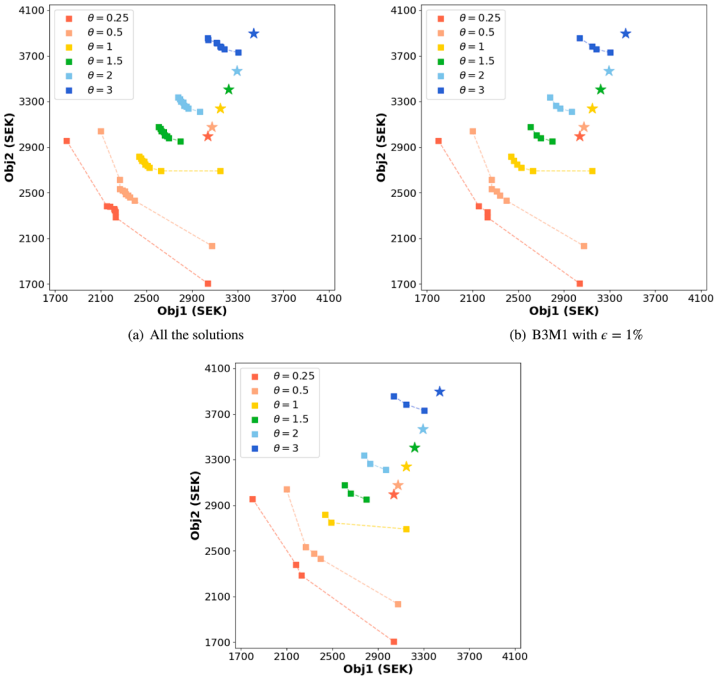

(a) All the solutions (b) B3M1 with $\epsilon = 1\%$

(c) B3M2 with $\epsilon = 1\%$

Fig. 17. Impact of changes in unit energy cost (θ) on optimized results using B3Ms.

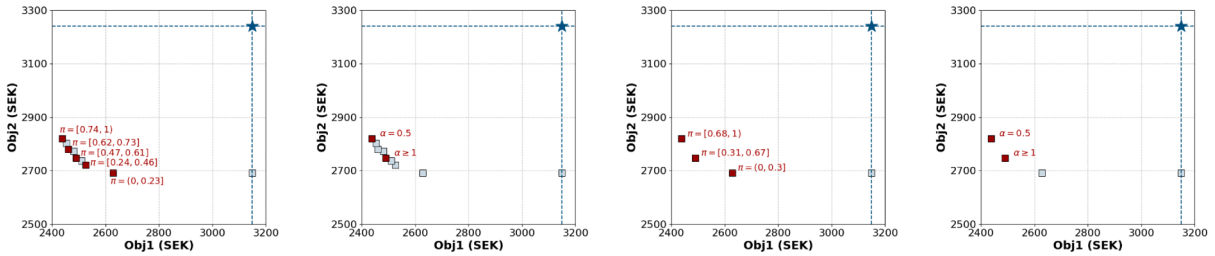

(a) Generalized Nash bargaining on all solutions (b) Distance function on all solutions (c) Generalized Nash bargaining on B3M1 with $\epsilon = 2\%$ (d) Distance function on B3M1 with $\epsilon = 2\%$

Fig. 18. Final solution of Case #1 with different methods.

the objectives are more aligned, both methods converge to nearly identical solutions, confirming the robustness of the representative frontier and its reduced sensitivity to parameterization. Overall, the two formulations provide complementary perspectives: the Nash rule highlights proportional fairness through explicit power settings, while the α-norm rule offers robustness-oriented selection. Their complementarity enables more reliable and interpretable choices, especially when the two objectives are closely aligned.

5.3.5. Charging scheduling results

Fig. 21 illustrates the spatiotemporal distribution of the optimized charging schedules for Case #3 ($\pi = [0.4 - 0.48]$ or $\alpha \geq 3$) using B3M1. The results demonstrate how EVs from each company are allocated to specific charging stations during defined time intervals, ensuring that the charging sessions fall within their designated charging TWs. The colors green and orange represent Company 1 and Company 2, respectively, while the "X" markers indicate the positions of the EVs.

As shown in Fig. 21, the optimization results indicate that only two charging stations are rented, a direct result of the high rental costs. EVs from Company 2 are predominantly served by the left-side charging station, while those from Company 1 primarily use the right-side charging station. This preference is attributable to the fact that charging at their own rented stations entails lower electricity costs than using other stations, which is in accordance with the cost-minimization objective of the model. The result reflects a rational self-prioritization mechanism that naturally emerges when companies face asymmetric rental costs.

Notably, the charging window - TW coupling reveals that most EVs begin charging at the start of their respective TWs. This behavior is driven by the incorporation of waiting time costs into the objective function, which motivates the results to minimize delays. The coupling shows that the model works well at making scheduling decisions that are in line with time constraints, which

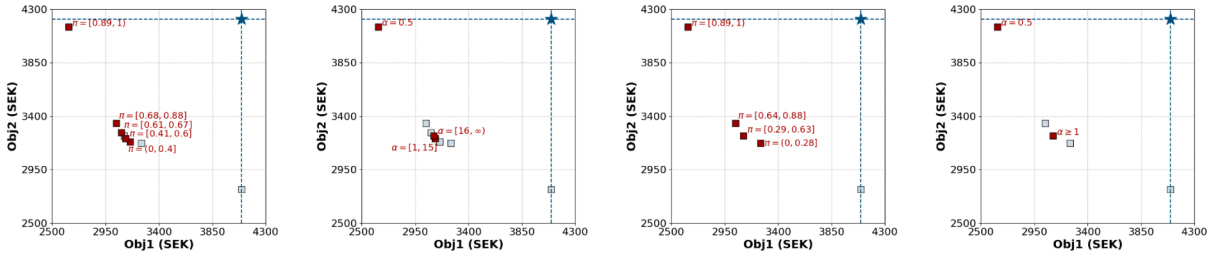

(a) Generalized Nash bargaining on all solutions

(b) Distance function on all solutions

(c) Generalized Nash bargaining on B3M1 with $\epsilon = 2\%$

(d) Distance function on B3M1 with $\epsilon = 2\%$

Fig. 19. Final solution of Case #2 with different methods.

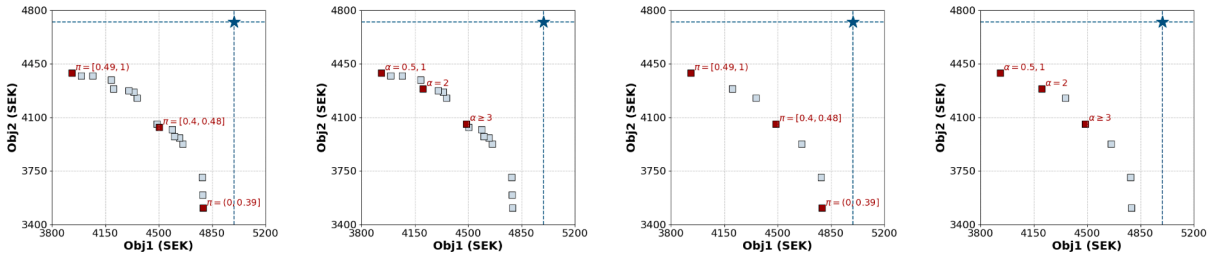

(a) Generalized Nash bargaining on all solutions

(b) Distance function on all solutions

(c) Generalized Nash bargaining on B3M1 with $\epsilon = 2\%$

(d) Distance function on B3M1 with $\epsilon = 2\%$

Fig. 20. Final solution of Case #3 with different methods.

increases its usefulness in real life. This synchronization behavior further illustrates how time-based incentives can drive spontaneous coordination among independent fleets, ensuring high resource utilization without explicit communication.

The results show that the proposed model efficiently allocates charging resources and resolves potential conflicts. The absence of overlapping charging assignments and optimal utilization of charging stations demonstrates this. Beyond ensuring feasible operation, these results reveal an implicit coordination mechanism that emerges from the joint optimization of rental and scheduling decisions. The fleets self-organize into non-overlapping usage patterns purely through cost and time incentives, suggesting that transparent pricing and shared-access rules could achieve comparable coordination in real-world multi-operator charging systems. These findings highlight the robustness of the optimization strategy in addressing the charging demands of both companies, offering valuable insights for designing collaborative charging management frameworks that balance autonomy and efficiency.

The following section discusses these findings in a broader context, highlighting their methodological implications and managerial relevance for collaborative EV charging systems.

6. Discussion

6.1. Algorithmic trade-offs

The results across all analyses collectively demonstrate how the proposed bi-objective optimization framework balances computational tractability, fairness, and operational efficiency in collaborative EV charging scheduling. The analyses reveal two consistent patterns. First, increasing the tolerance range (ϵ) in the B3Ms significantly reduces computational time while maintaining solution accuracy up to a practical limit, as all retained points are exact and lie on the exact non-dominated frontier. This trade-off between precision and efficiency reflects companies' willingness to tolerate minor profit deviations in exchange for faster decision-making, suggesting that the tolerance range can be interpreted as a quantitative indicator of acceptable flexibility in real-world negotiations. Second, B3M1 and B3M2 present a trade-off between frontier completeness and computational efficiency. Both methods filter out solutions that are close in objective space, but B3M2 applies a stricter dominance criterion, resulting in fewer retained points and faster computation. The choice between them ultimately depends on whether decision-makers prioritize comprehensive frontier coverage or reduced computational effort.

6.2. Behavioral sensitivity

The observed sensitivity patterns further highlight how behavioral and market parameters jointly influence the benefits of collaboration. Higher VOT amplifies the relative advantage of cooperative scheduling by increasing the penalty of waiting, whereas higher energy costs reduce these gains by narrowing cost differentials between fleets. This interaction suggests that the incentive for collaboration is driven more by time valuation than by energy price levels. Operators with tighter schedules have stronger motivation to

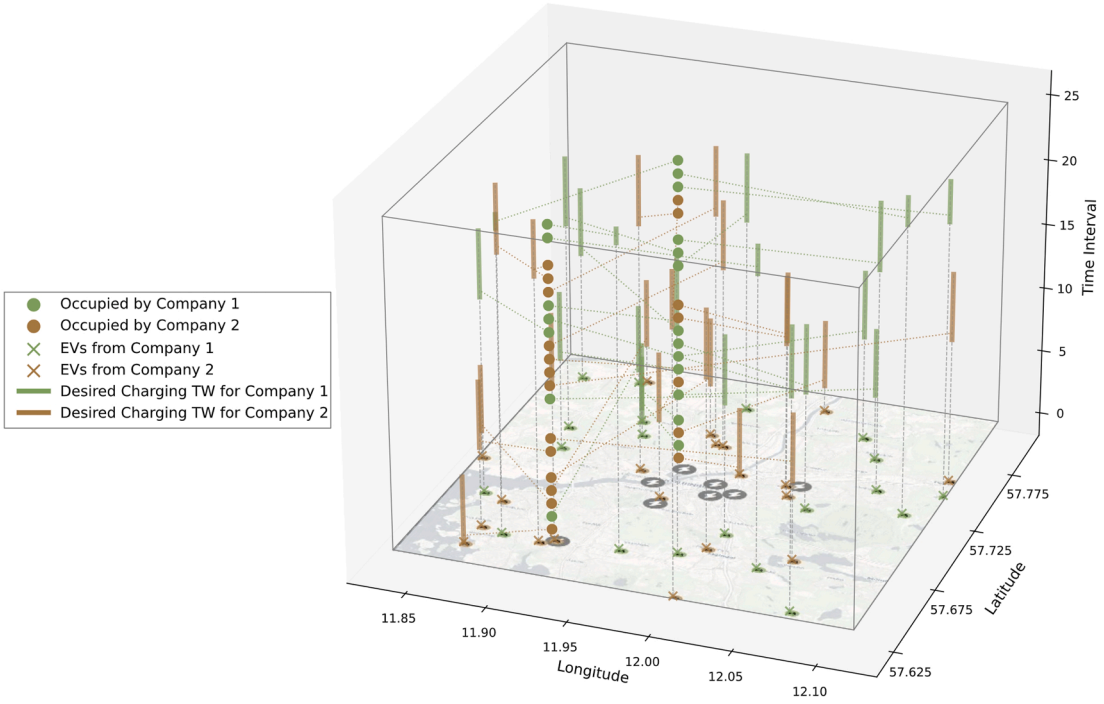

Fig. 21. Spatiotemporal distribution of EV charging scheduling results.

coordinate, whereas uniform or elevated energy prices may undermine cooperative behavior. Recognizing this behavioral sensitivity is crucial for designing pricing schemes or contractual rules that sustain long-term collaboration. Interestingly, several non-dominated points remain overlapping across different VOT levels, indicating the existence of stable compromise regions where trade-offs between the objectives are relatively insensitive to behavioral changes. These robust solutions suggest that decision-makers can identify operating points that remain effective under varying user valuations, providing practical guidance for both long-term scheduling and pricing policies, as well as for the design of stable coordination rules in shared charging systems. In addition, the convergence between the Nash bargaining and α-norm methods across different cases suggests that fairness-oriented outcomes remain stable under varying decision representations, providing complementary perspectives for balancing efficiency and equity in multi-stakeholder systems.

6.3. Operational aspects

At the operational level, the charging scheduling results illustrate how the joint optimization of station rental and temporal allocation naturally yields conflict-free, high-utilization patterns. This outcome indicates that effective coordination can emerge purely from cost and time incentives, without requiring explicit communication between operators. Moreover, the cooperative bargaining process transforms a purely algorithmic optimization into a transparent and equitable decision mechanism. By making the reasoning behind the final solution interpretable to all participants, it enhances mutual trust and lowers negotiation uncertainty, both of which are essential for sustaining long-term collaboration. From a management perspective, these insights suggest that transparent pricing schemes and adjustable tolerance ranges could be used as governance levers to balance autonomy and cooperation in shared charging networks, while the proposed framework demonstrates strong interpretability and computational efficiency by bridging algorithmic performance with managerial transparency. These characteristics make it a promising foundation for future extensions toward real-time, adaptive, and data-informed decision systems.

Operationally, the proposed framework provides clear decision levers for charging system operators under different coordination contexts. The tolerance range ϵ can be interpreted as an explicit flexibility parameter that reflects operators' willingness to accept minor profit deviations in exchange for reduced computational effort and faster coordination. For long-term planning or offline analysis, a smaller tolerance supports more complete exploration of the Pareto frontier, whereas in time-sensitive or large-scale operational settings, a larger tolerance enables rapid decision-making without sacrificing solution optimality within a practical margin. Similarly, the contrast between B3M1 and B3M2 highlights a trade-off between frontier completeness and computational efficiency, suggesting that B3M1 is better suited for strategic assessment, while B3M2 is more appropriate for operational deployment where responsiveness and computational efficiency are prioritized. These interpretations translate the algorithmic design choices into actionable guidance for operators facing different planning horizons and system constraints.

6.4. Implementation consideration

From a practical deployment perspective, the results also highlight several considerations relevant to real-world charging systems. The observed sensitivity to the value of time (VOT) suggests that collaborative charging is particularly beneficial in contexts with tight schedules or high opportunity costs, such as commercial fleets or urban delivery operations, whereas uniformly high energy prices alone may not be sufficient to sustain strong cooperation incentives. In addition, while the proposed framework assumes transparent information exchange to support cooperative bargaining, real-world implementations may face coordination costs, limited information sharing, or heterogeneous market power across operators. Acknowledging these frictions does not diminish the value of the framework, but rather clarifies the conditions under which it is most effective and where institutional or contractual support may be required. These insights reinforce the relevance of the proposed approach for transportation systems that aim to balance efficiency, fairness, and operational feasibility in shared charging environments, and they also suggest that successful implementation may depend on supportive governance arrangements for transparency, coordination, and data sharing.

Several implementation challenges may arise when translating the proposed framework into real-world charging systems. First, although the proposed framework targets operational coordination among EV fleet operators that have already established a collaborative relationship, its effectiveness in practice may still depend on sustained trust and repeated interaction during day-to-day operation. Willingness to comply with agreed schedules, perceptions of fairness, and confidence in information transparency can influence the stability and long-term performance of collaborative scheduling mechanisms in real-world operations. Second, while the proposed framework assumes that agreed charging schedules can be executed as planned, real-world operations may experience deviations due to delayed arrivals, extended charging durations, or unforeseen operational disruptions. In this regard, the use of relatively coarse time slots in the model already provides a degree of flexibility, but practical implementations may benefit from incorporating additional buffers or redundancy to enhance robustness. In addition, extending the framework to multi-operator coordination and adapting it to dynamic demand or pricing conditions would require additional institutional or algorithmic support. Finally, information availability and alignment across operators remain a practical consideration, particularly in competitive environments where data sharing and standardization are not guaranteed. These challenges do not undermine the proposed approach, but rather highlight complementary institutional and operational considerations that are important for successful deployment.

7. Conclusion

This paper addresses the collaborative scheduling problem in which two companies share charging stations, utilizing a bi-objective optimization approach to minimize costs for both parties through a collaborative scheduling model. We develop B3Ms to efficiently generate a representative subset of globally optimal solutions with substantially reduced computational effort. Furthermore, the Nash bargaining approach is used to ensure equitable cooperation between the companies. Overall, the proposed bi-objective model and developed methods demonstrate their versatility and applicability for planning-oriented collaborative charging problems, contributing to the advancement of sustainable urban logistics through horizontal collaboration.

The B3Ms proposed in this study are applicable to a broad class of bi-objective integer programming models. These methods are promising because they can significantly reduce computational time while preserving the structure of the efficient frontier. We introduced two distinct methods: the first is more conservative, involving searching for a solution within a defined rectangle and disregarding those that are very similar to existing solutions. In contrast, the second method is more aggressive, directly shrinking the rectangular space to eliminate certain solutions. While the aggressive method may miss some solutions compared to the conservative one, leading to gaps around the predetermined tolerance range, it is more efficient in terms of computational time. The conservative method maintains solutions well within the tolerance range, sometimes even tighter.

In addition, the cooperative bargaining method we propose can be broadly applied to all bi-objective programming models to identify the final agreement point. Although the two approaches differ in their proximity to key reference points, they ultimately converge toward the same direction: one method is positioned farther from the non-dominated point, while the other is closer to the ideal point. The two companies can set parameter values, such as power, and negotiate to reach the final solution.

Beyond computational advantages, the integration of the B3Ms and cooperative bargaining components contributes to transparent and equitable decision-making. Each operator can clearly interpret how trade-offs are negotiated and how the final scheduling solution is reached, ensuring procedural fairness and reinforcing confidence in the collaboration process. Such transparency is crucial for establishing durable cooperative relationships in shared-charging operations, where long-term trust often determines the success of joint infrastructure use.

The findings also carry several policy implications. First, improving the performance of shared charging systems is not only a matter of adding charging capacity, but also of designing coordination mechanisms that align incentives among operators while maintaining fairness and transparency. Second, because the gains from collaboration appear to be more sensitive to value-of-time conditions than to energy prices alone, public policies and platform rules should not rely solely on uniform price signals, but may instead benefit from more context-sensitive or behavior-aware coordination mechanisms. Third, the stability of several compromise solutions across different behavioral settings suggests that planners and regulators may promote robust charging arrangements that remain effective and acceptable under heterogeneous operator preferences. Finally, the practical deployment of collaborative charging is likely to benefit from institutional support, such as data-sharing standards, contractual coordination, and governance rules that reduce coordination costs and build trust among participating operators.

Several promising directions remain open for further research. First, addressing increasingly large problem instances remains a practical challenge, as even a reduced set of exact representative solutions may become computationally intensive. Developing region-

wise decomposition strategies or distributed versions of B3Ms could improve tractability while preserving solution interpretability and structural properties. Second, extending the framework to incorporate real-time operational uncertainties, such as unpredictable vehicle arrivals, dynamic fleet participation, and fluctuations in station availability, would improve the robustness and adaptability of the scheduling framework under realistic conditions. Third, extending the model to accommodate interruptive scheduling behaviors, where EVs may be preempted, reassigned, or rescheduled in response to operational disruptions or shifting priorities, would further increase its flexibility and practical relevance in complex fleet operations. Finally, integrating lightweight AI-based decision-support tools that learn company-level preferences or contextual features could assist autonomous solution selection, enhancing the framework's intelligence while maintaining its decentralized and fair nature. These directions collectively aim to improve computational tractability and robustness while extending the framework toward increasingly dynamic and uncertain transportation environments.

CRediT authorship contribution statement

Fangting Zhou: Writing – review & editing, Writing – original draft, Visualization, Validation, Software, Methodology, Investigation, Formal analysis, Data curation, Conceptualization; **Balázs Kulcsár:** Writing – review & editing, Validation, Supervision, Project administration, Methodology, Funding acquisition, Conceptualization; **Jiaming Wu:** Writing – review & editing, Methodology, Formal analysis, Data curation.

Acknowledgments

This work was supported by the European Commission and the Swedish Energy Agency through the project E-Laas (F-ENUAC-2022-0003). The authors also appreciate the support of the project ERGODIC (F-DUT-2022-0078) funded by the European Commission and Vinnova. Finally, the project LEAR: Robust LEArning methods for electric vehicle route selection sponsored by the Swedish Electromobility Center is also acknowledged.

Appendix A.

The notations used for all the solution approaches can be found in Table A1.

Table A1
Notations for solution approaches.

Symbol	Description
$\mathcal{X}, \mathcal{Z}$	Set of solutions and corresponding objective function values, where $x \in \mathcal{X}$ and $z \in \mathcal{Z}$
$\tilde{\mathcal{X}}$	Reduced set of solutions, where $\tilde{\mathcal{X}} \subset \mathcal{X}$
x, z	A specific solution and its corresponding objective function value, where $z = z(x)$, and x represents the combination of decision variables (x_{ij}^r, y_j^k)
x^*, z^*	Final solution and its corresponding objective function value
z^T, z^B	The top and bottom points of the efficient frontier
z_k	Objective function k
z_1, z_2	The first and second objective functions, where $z(x) = \left(z_1(x), z_2(x)\right)$
$C_k^{\min}$	Cost threshold of company k
z^{Non}	Non-collaborative point
z^t, z^b	Points to define the top and bottom rectangles
$z^{n,1}, z^{n,2}$	New solutions found in the bottom rectangle and top rectangle
$R(z^T, z^B)$	The rectangle defined by the top-left point z^T and the bottom-right point z^B
R^T, R^B	Top and bottom rectangles
$\mathcal{Z}^e$	The set of objective function values corresponding to the existing solutions, where $z^e \in \mathcal{Z}^e$
z^e	Existing solution
z^n	New solution
σ_1, σ_2	Tolerance margins for objectives 1 and 2
ϵ	Tolerance range, expressed as a percentage
ζ	A small constant

Appendix B.

The flowchart for the balanced box method is illustrated in Fig. B1. This method revolves around the exploration of rectangles and comprises four main steps. A comprehensive explanation of these steps is provided below, offering further clarification on the operations in the flowchart.

Step 1: To identify a yet unidentified non-dominated point, it is necessary to divide the rectangle $R(z^T, z^B)$ into two distinct regions, the top rectangle (R^T) and the bottom rectangle (R^B). These two rectangles are defined by the points z^T, z^t, z^b, and z^B. In this case, the value of z^t is $(z_1^B, (z_2^T + z_2^B)/2)$, while z^b is $(z_1^T, (z_2^T + z_2^B)/2)$. In other words, the original rectangle is divided horizontally along the $z_2(x)$ axis, and subsequently removed from the rectangle set.

Step 2: The lower rectangle, $R^B(z^b, z^B)$, can be searched by solving the following optimization problem: $\text{lexmin}_{x \in \mathcal{X}} \left\{z_1(x), z_2(x) : z(x) \in R^B\right\}$. If a new non-dominated point is found, then a portion of the rectangle $R^T(z^T, z^t)$ is

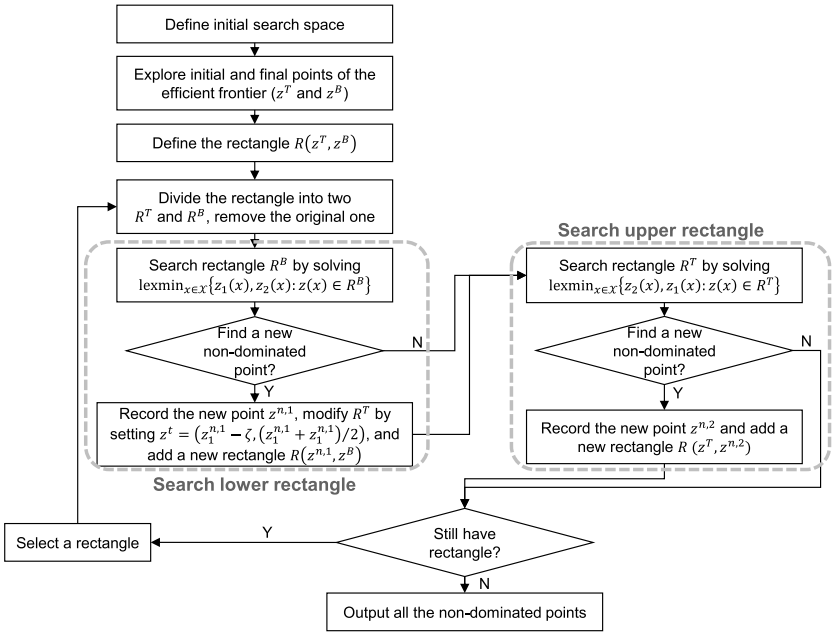

Fig. B1. The flowchart of the balanced box method.

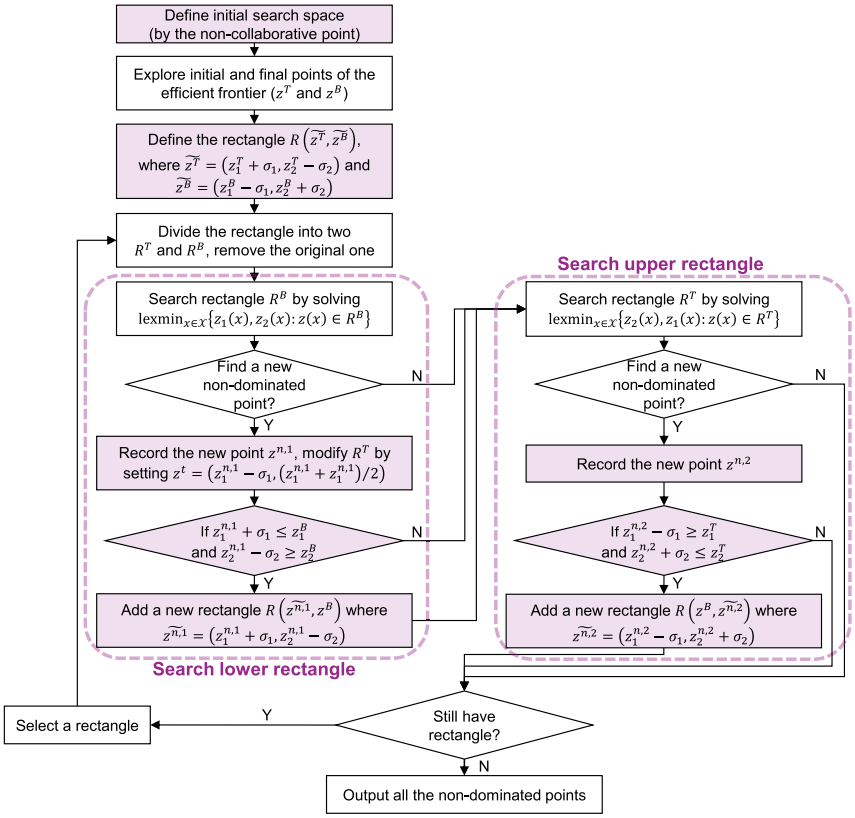

Fig. B2. The flowchart of B3M2.

dominated. The rectangle $R^T(z^T, z^t)$ should be modified by setting z^t equal to $(z_1^{n,1} - \zeta, (z_2^T + z_2^B)/2)$, where ζ is a small constant. Furthermore, a new rectangle, $R(z^{n,1}, z^B)$, should be incorporated into the existing rectangle set. The non-dominated point is then recorded. If no new solution is identified, $R^T(z^T, z^t)$ remains unchanged, and no further rectangle is incorporated.

Step 3: The upper rectangle, $R^T(z^T, z^t)$, can be searched by solving the following optimization problem: $\text{lexmin}_{x\in\mathcal{X}} \{z_2(x), z_1(x) : z(x) \in R^T\}$. If a new non-dominated point is identified, then a new rectangle, $R(z^T, z^{n,2})$, should be incorporated into the existing rectangle set. The non-dominated point is then recorded; otherwise, no new rectangle is included.

Step 4: If the rectangle set is not empty, a single rectangle should be selected from the set, and the procedure proceeds to Step 1; otherwise, all the non-dominated points are output.

Fig. B2 details the B3M2 procedure, where purple boxes mark revised or newly added steps relative to Fig. B1. The principal change is the rectangle redefinition.

Appendix C.

To analyze the general properties of the α-norm, we derive its upper and lower bounds based on the parameter α. Specifically, the bounds for $\|f(z)\|_\alpha$ are given by:

$$\left(\sum_{i=1}^{n} |f(z_i)|^\alpha\right)^{1/\alpha} \le \left(\sum_{i=1}^{n} \left|\max_i f(z_i)\right|^\alpha\right)^{1/\alpha} = n^{1/\alpha} \max_i |f(z_i)|, \tag{C1}$$

and

$$\left(\sum_{i=1}^{n} |f(z_i)|^\alpha\right)^{1/\alpha} \ge \left(\max_i |f(z_i)|^\alpha\right)^{1/\alpha} = \max_i |f(z_i)|. \tag{C2}$$

These bounds establish the range of the α-norm, illustrating its confinement between the maximum individual value and a scaled aggregation determined by α. According to Eqs. (C1) and (C2), $\|f(z)\|_\alpha$ limits by:

$$\max_i |f(z_i)| \le \|f(z)\|_\alpha \le n^{1/\alpha} \max_i |f(z_i)|. \tag{C3}$$

As α approaches ∞, the p-norm approaches the infinity norm or maximum norm. This behavior highlights how the ∞-norm emphasizes the largest deviation, making it particularly suitable for robust optimization problems.

$$\|f(z)\|_\infty := \max_i |f(z_i)| = \max_i \left|\frac{z_i - \underline{z}_i}{\overline{z}_i - \underline{z}_i}\right|, \tag{C4}$$

the corresponding Nash bargaining solution is:

$$s^* = \operatorname*{argmin}_{z\in\mathcal{Z}} \|f(z)\|_\infty := \operatorname*{argmin}_{z_i\in\mathcal{Z}} \left(\max_i \left|\frac{z_i - \underline{z}_i}{\overline{z}_i - \underline{z}_i}\right|\right). \tag{C5}$$

Based on the properties of the ∞-norm, Eq. (C5) formulates a min-max optimization problem, which is commonly used to handle worst-case scenarios. This approach is commonly used in equilibrium problems and robust optimization. Overall, the α-norm framework provides a flexible framework to measure distances, ranging from the Manhattan norm ($\alpha = 1$) to the Euclidean norm ($\alpha = 2$), and ultimately to the maximum norm ($\alpha \to \infty$), each offering unique properties for different sensitivities in optimization problems.

References

ABB News Center, 2021. Abb invests in e-mobility startup go to-u. https://new.abb.com/news/detail/82687/abb-invests-in-e-mobility-startup-go-to-u. Describes reservation capability; Accessed: 2025-10-28.

ACEA, 2022. A European EV Charging Infrastructure Masterplan. Technical Report. European Automobile Manufacturers' Association (ACEA). Accessed: 2025-02-20. https://www.acea.auto/files/Research-Whitepaper-A-European-EV-Charging-Infrastructure-Masterplan.pdf.

Bauer, G., Hsu, C.-W., Nicholas, M., Lutsey, N., 2021. Charging up America: Assessing the Growing Need for US Charging Infrastructure Through 2030. White Paper ICCT https://theicct.org/sites/default/files/publications/charging-up-america-jul2021.pdf.

Boland, N., Charkhgard, H., Savelsbergh, M., 2015. A criterion space search algorithm for biobjective integer programming: the balanced box method. INFORMS J. Comput. 27 (4), 735–754. https://doi.org/10.1287/ijoc.2015.0657

Cai, Z., Li, C., Mo, D., Xu, S., Chen, X.M., Lee, D.-H., 2024. Optimizing consolidated shared charging and electric ride-sourcing services. Transp. Res. E: Logist. Transp. Rev. 184, 103484. https://doi.org/10.1016/j.tre.2024.103484

Chen, B., Chen, Z., Liu, X.C., Yi, Z., 2024. Bayesian inference-based spatiotemporal modeling with interim activities for EV charging etiquette. Transp. Res. D: Transp. Environ. 127, 104060. https://doi.org/10.1016/j.trd.2024.104060

Co Charger, 2025. Host calculator. https://co-charger.com/host-calculator/. Accessed: 2025-02-04.

Dai, R., Charkhgard, H., 2018. A two-stage approach for bi-objective integer linear programming. Oper. Res. Lett. 46 (1), 81–87. https://doi.org/10.1016/j.orl.2017.11.011

Das, R., Wang, Y., Putrus, G., Kotter, R., Marzband, M., Herteleer, B., Warmerdam, J., 2020. Multi-objective techno-economic-environmental optimisation of electric vehicle for energy services. Appl. Energy 257, 113965. https://doi.org/10.1016/j.apenergy.2019.113965

European Alternative Fuels Observatory, 2024. Electric vehicle recharging prices. https://alternative-fuels-observatory.ec.europa.eu/markets-and-policy/market-and-consumer-insights/electric-vehicle-recharging-prices. Accessed: 2026-02-10.

EVgo Press Office, 2021. Evgo launches Reservations at fast charging stations in three markets. https://www.evgo.com/press-release/evgo-reservations-launches-at-fast-charging-stations-3-markets/. Accessed: 2025-10-28.

Fröde, P., Lee, M., Sahdev, S., 2023. Can public EV fast-charging stations be profitable in the United States? McKinsey Co. Insight. Accessed: 2025-02-15. https://www.mckinsey.com/features/mckinsey-center-for-future-mobility/our-insights/can-public-ev-fast-charging-stations-be-profitable-in-the-united-states.
Gao, J., Wong, T., Wang, C., Yu, J.Y., 2021. A price-based iterative double auction for charger sharing markets. IEEE Trans. Intell. Transp. Syst. 23 (6), 5116–5127. https://doi.org/10.1109/TITS.2020.3047984
Hajforoosh, S., Masoum, M. A.S., Islam, S.M., 2015. Real-time charging coordination of plug-in electric vehicles based on hybrid fuzzy discrete particle swarm optimization. Electr. Power Syst. Res. 128, 19–29. https://doi.org/10.1016/j.epsr.2015.06.019
IEA, 2025. Global EV Outlook 2025: Expanding Sales in Diverse Markets. Technical Report. International Energy Agency. Accessed: 2026-04-04. https://www.iea.org/reports/global-ev-outlook-2025.
Ji, J., Bie, Y., Wang, L., 2023. Optimal electric bus fleet scheduling for a route with charging facility sharing. Transp. Res. C: Emerg. Technol. 147, 104010. https://doi.org/10.1016/j.trc.2022.104010
Jia, Z., An, K., Ma, W., 2024. Utilizing electric bus depots for public charging: operation strategies and benefit analysis. Transp. Res. D: Transp. Environ. 130, 104155. https://doi.org/10.1016/j.trd.2024.104155
Kampshoff, P., Kumar, A., Peloquin, S., Sahdev, S., 2022. Building the electric-vehicle charging infrastructure America needs. Technical Report. New York, NY: McKinsey & Company. Accessed: 2025-02-17. https://www.mckinsey.com/industries/public-sector/our-insights/building-the-electric-vehicle-charging-infrastructure-america-needs.
Kumar, R.R., Chakraborty, A., Mandal, P., 2021. Promoting electric vehicle adoption: who should invest in charging infrastructure? Transp. Res. E: Logist. Transp. Rev. 149, 102295. https://doi.org/10.1016/j.tre.2021.102295
Laidoui, F., Bessedik, M., Tayeb, F. B.-S., 2023. A game-theoretical constructive approach for the multi-objective frequency assignment problem. Appl. Soft Comput. 144, 110444. https://doi.org/10.1016/j.asoc.2023.110444
Levinson, R.S., West, T.H., 2018. Impact of public electric vehicle charging infrastructure. Transp. Res. D: Transp. Environ. 64, 158–177. https://doi.org/10.1016/j.trd.2017.10.006
Liu, X., Liu, X.C., Liu, Z., Shi, R., Ma, X., 2023a. A solar-powered bus charging infrastructure location problem under charging service degradation. Transp. Res. D: Transp. Environ. 119, 103770. https://doi.org/10.1016/j.trd.2023.103770
Liu, Y., Francis, A., Hollauer, C., Lawson, M.C., Shaikh, O., Cotsman, A., Bhardwaj, K., Banboukian, A., Li, M., Webb, A., et al., 2023b. Reliability of electric vehicle charging infrastructure: a cross-lingual deep learning approach. Commun. Transp. Res. 3, 100095. https://doi.org/10.1016/j.commtr.2023.100095
Melander, L., Wallström, H., 2023. The benefits of green horizontal networks: lessons learned from sharing charging infrastructure for electric freight vehicles. Bus. Strategy Environ. 32 (4), 1835–1846. https://doi.org/10.1002/bse.3222
Nash, J., 1953. Two-person cooperative games. Econometrica 21 (1), 128–140. https://doi.org/10.2307/1906951
Nord Pool, 2024. Nord pool. https://www.nordpoolgroup.com. Accessed: 2026-04-05.
openrouteservice, 2024. Openrouteservice matrix service. Accessed: 2025-02-05. https://openrouteservice.org/dev/#/api-docs/v2/matrix/%7Bprofile%7D/post.
Smet, P., 2023. Generating balanced workload allocations in hospitals. Oper. Res. Health Care 38, 100390. https://doi.org/10.1016/j.orhc.2023.100390
Vanrykel, F., Ernst, D., Bourgeois, M., 2018. Fostering share&charge through proper regulation. Compet. Regul. Netw. Ind. 19 (1-2), 25–52. https://doi.org/10.1177/1783591718809576
Wang, T., Du, Y., Fang, D., Li, Z.-C., 2020. Berth allocation and quay crane assignment for the trade-off between service efficiency and operating cost considering carbon emission taxation. Transp. Sci. 54 (5), 1307–1331. https://doi.org/10.1287/trsc.2019.0946
Wei, Z., Li, Y., Zhang, Y., Cai, L., 2017. Intelligent parking garage EV charging scheduling considering battery charging characteristic. IEEE Trans. Ind. Electron. 65 (3), 2806–2816. https://doi.org/10.1109/TIE.2017.2740834
Wu, H., Pang, G. K.-H., Choy, K.L., Lam, H.Y., 2017. A charging-scheme decision model for electric vehicle battery swapping station using varied population evolutionary algorithms. Appl. Soft Comput. 61, 905–920. https://doi.org/10.1016/j.asoc.2017.09.008
Wu, W., Lin, Y., Liu, R., Li, Y., Zhang, Y., Ma, C., 2020. Online EV charge scheduling based on time-of-use pricing and peak load minimization: properties and efficient algorithms. IEEE Trans. Intell. Transp. Syst. 23 (1), 572–586. https://doi.org/10.1109/TITS.2020.3014088
Yi, Z., Liu, X.C., Wei, R., 2022. Electric vehicle demand estimation and charging station allocation using urban informatics. Transp. Res. D: Transp. Environ. 106, 103264. https://doi.org/10.1016/j.trd.2022.103264
Yin, W., Ming, Z., Wen, T., 2021. Scheduling strategy of electric vehicle charging considering different requirements of grid and users. Energy 232, 121118. https://doi.org/10.1016/j.energy.2021.121118
Zakariazadeh, A., Jadid, S., Siano, P., 2014. Multi-objective scheduling of electric vehicles in smart distribution system. Energy Convers. Manag. 79, 43–53. https://doi.org/10.1016/j.enconman.2013.11.042
Zhang, Y., You, P., Cai, L., 2018. Optimal charging scheduling by pricing for EV charging station with dual charging modes. IEEE Trans. Intell. Transp. Syst. 20 (9), 3386–3396. https://doi.org/10.1109/TITS.2018.2876287
Zhou, F., Arvidsson, A., Wu, J., Kulcsar, B., 2024. Collaborative electric vehicle routing with meet points. Commun. Transp. Res. 4, 100135. https://doi.org/10.1016/j.commtr.2024.100135